Mapping the Cosmic Evolution of Fermi Blazars

Garima Rajguru, Clemson University

Lea Marcotulli, Yale University

Marco Ajello, Clemson University

Counting Experiment

What are we counting?

- **Blazars -** Jet points along our line of sight.
- Two types- FSRQs and BL Lacs.

How does counting give us information about evolution?

- Counting the number of objects per unit comoving volume and luminosity interval gives us the Luminosity Function (LF).

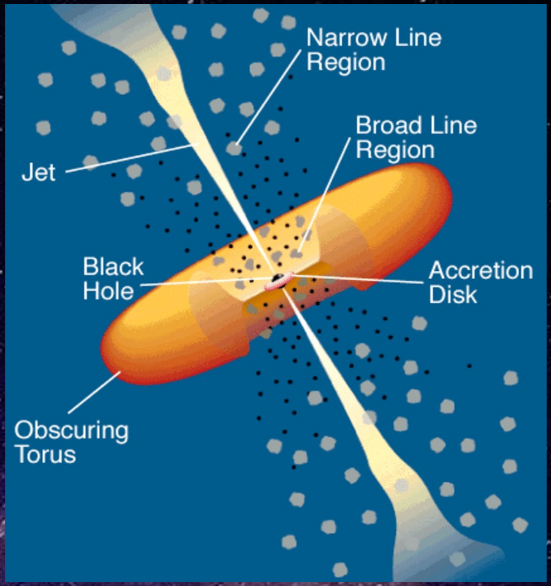

Urry and Padovani 1995

Luminosity Function of Blazars

Luminosity Function encodes evolution - Blazar LF is not well constrained

Blazars are good cosmological probes - High luminosities and large redshifts

Open Question - Do FSRQs and BL Lacs have the same evolution?

Application - Contribution of blazar emission to the extragalactic γ-ray background (EGB)

Cavaliere & D'Elia 2002.
Ajello et al. 2014. Ajello et al. 2015.

Dataset

2497 Sources from Fermi LAT 8-year Source List (Marcotulli 2020).

Larger than previous samples (Ajello+14/15 ~400). Would lead to remarkable improvement in LF determination.

100 MeV-1 TeV range. Extragalactic sources.

Classification	Number of sources
FSRQ	529
BL Lacs	1094
BCU	741

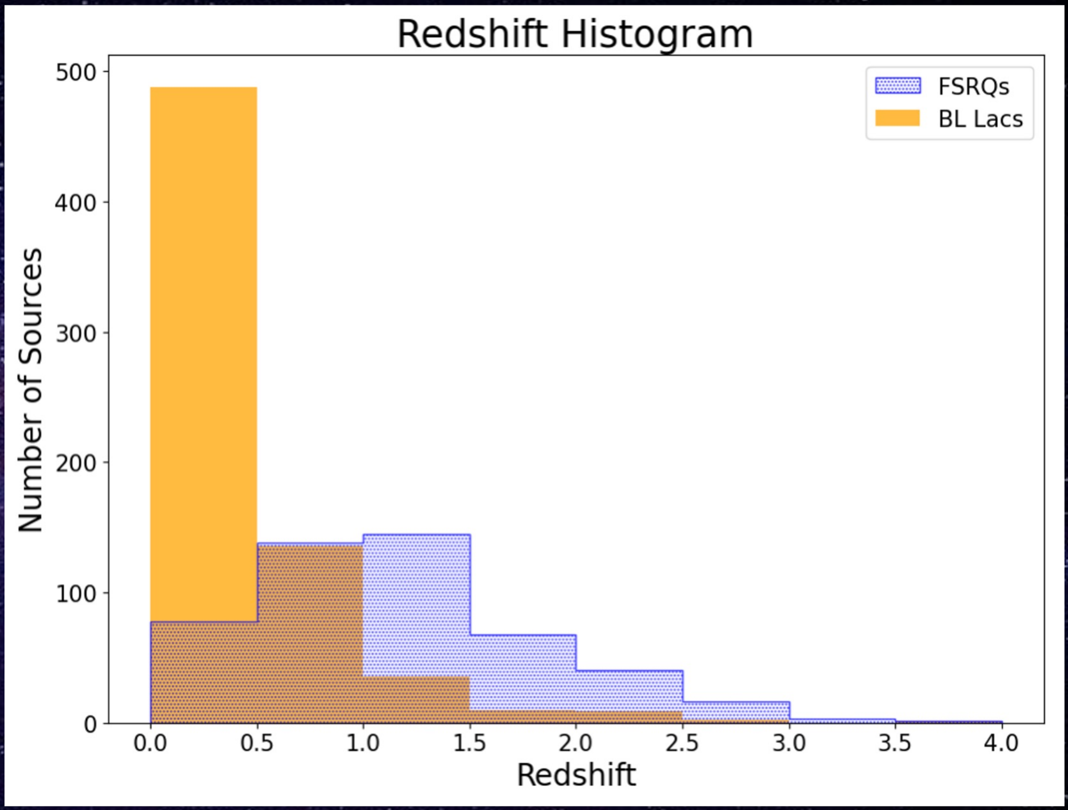

Marcotulli, L., Di Mauro, M. and Ajello, M., 2020.

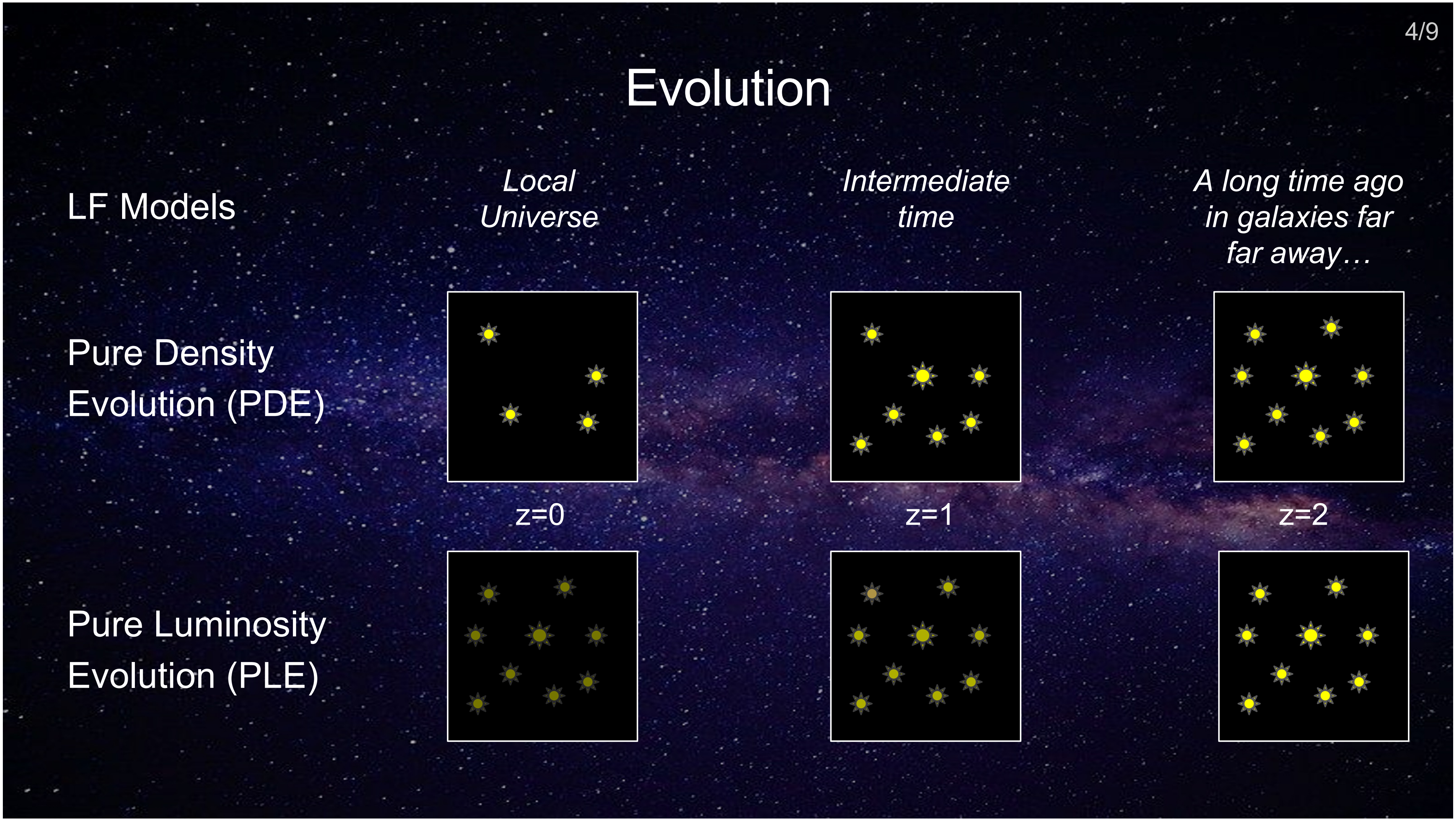
4/9
Evolution
LF Models
Local Universe
Intermediate time
A long time ago in galaxies far far away…
Pure Density Evolution (PDE)
z=0
z=1
z=2
Pure Luminosity Evolution (PLE)

Luminosity Function at z=0

- Best-fit LF has double PL shape.
- Spans 4 orders of magnitude lower than previous studies.

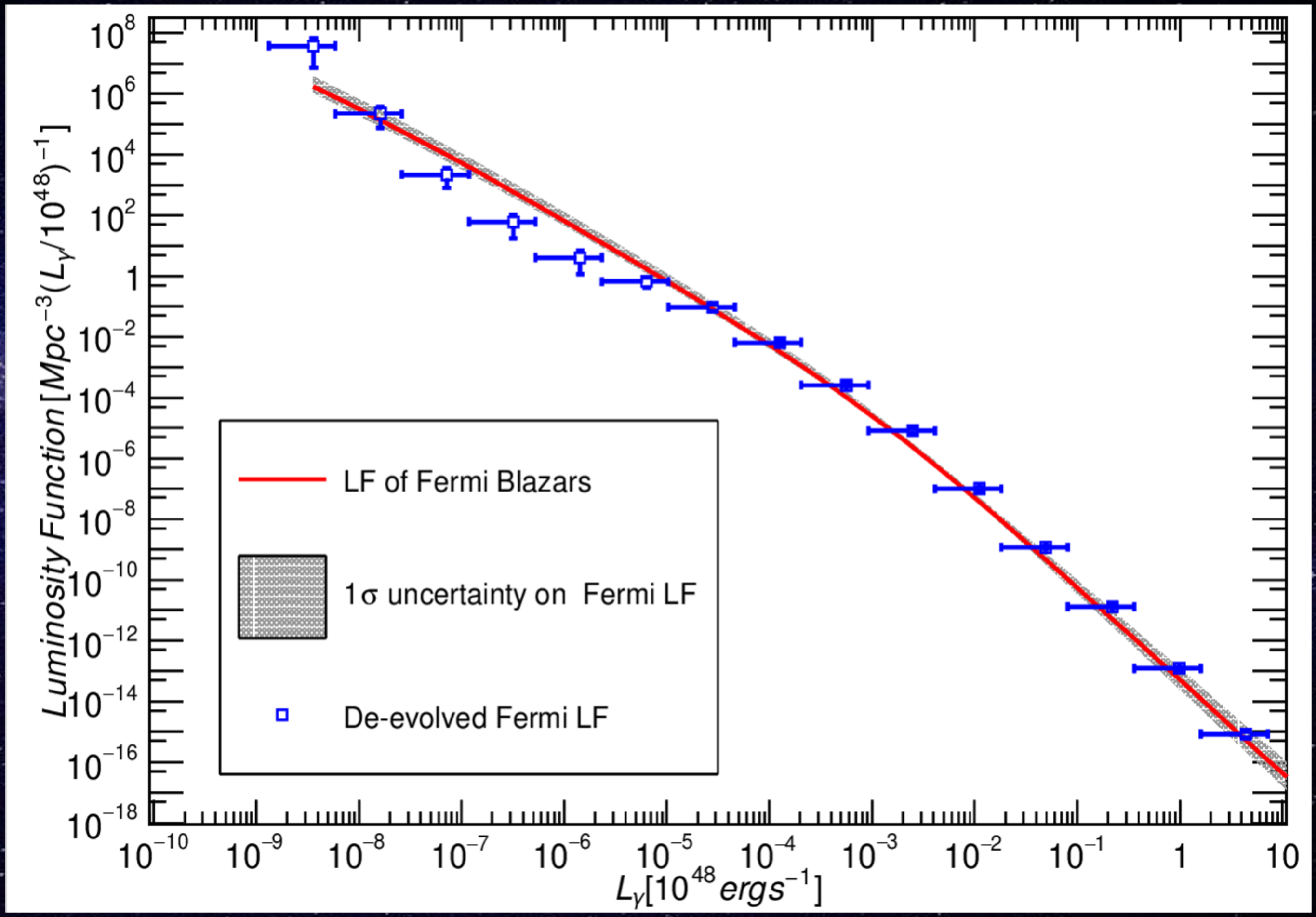

Evolution of Luminosity Function

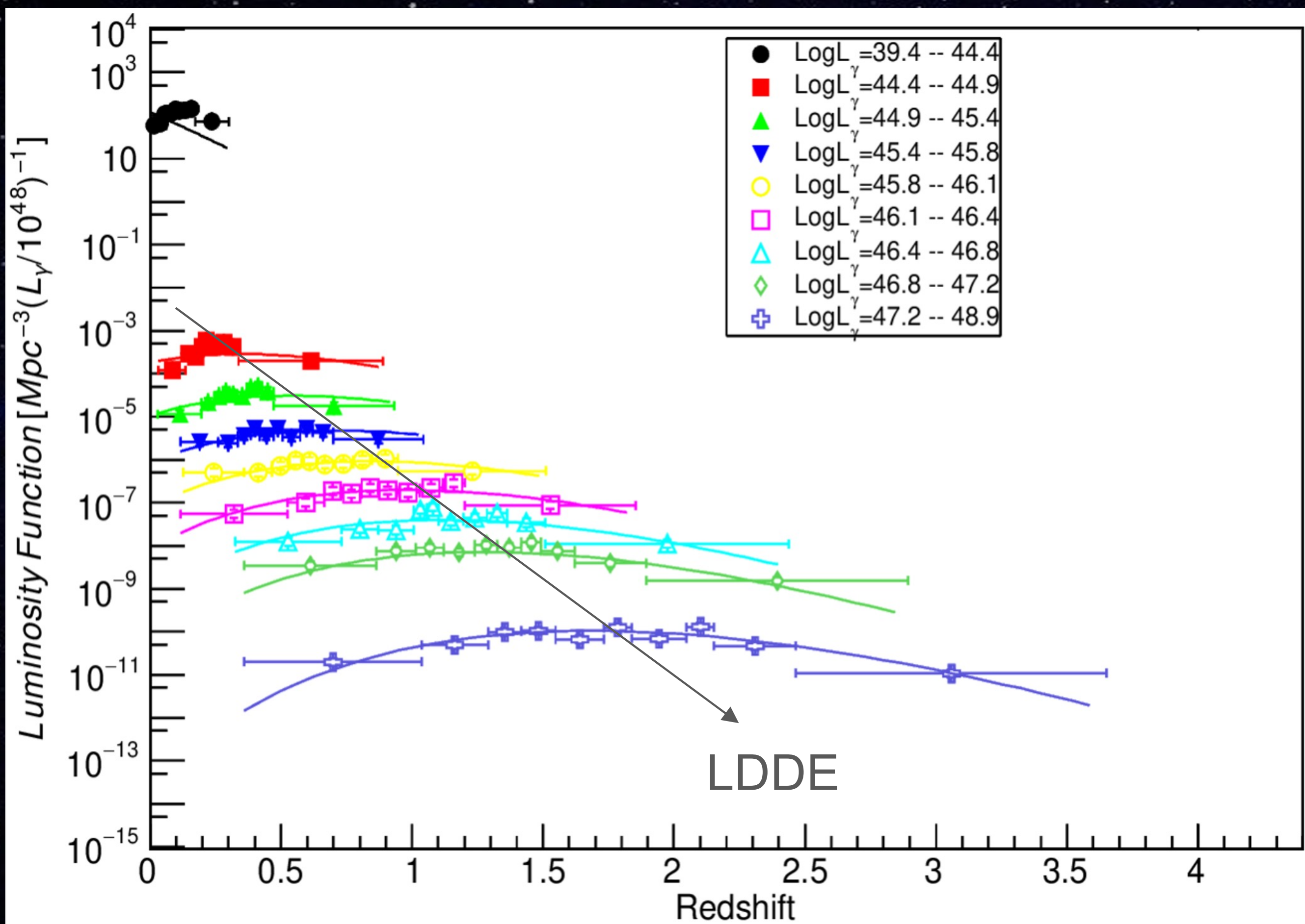

- Luminosity Dependent Density Evolution (LDDE).
- Luminous sources evolve positively.

Space Density of Blazars

Change in curvature of density plot can hint towards the link between FSRQs and BL Lacs.

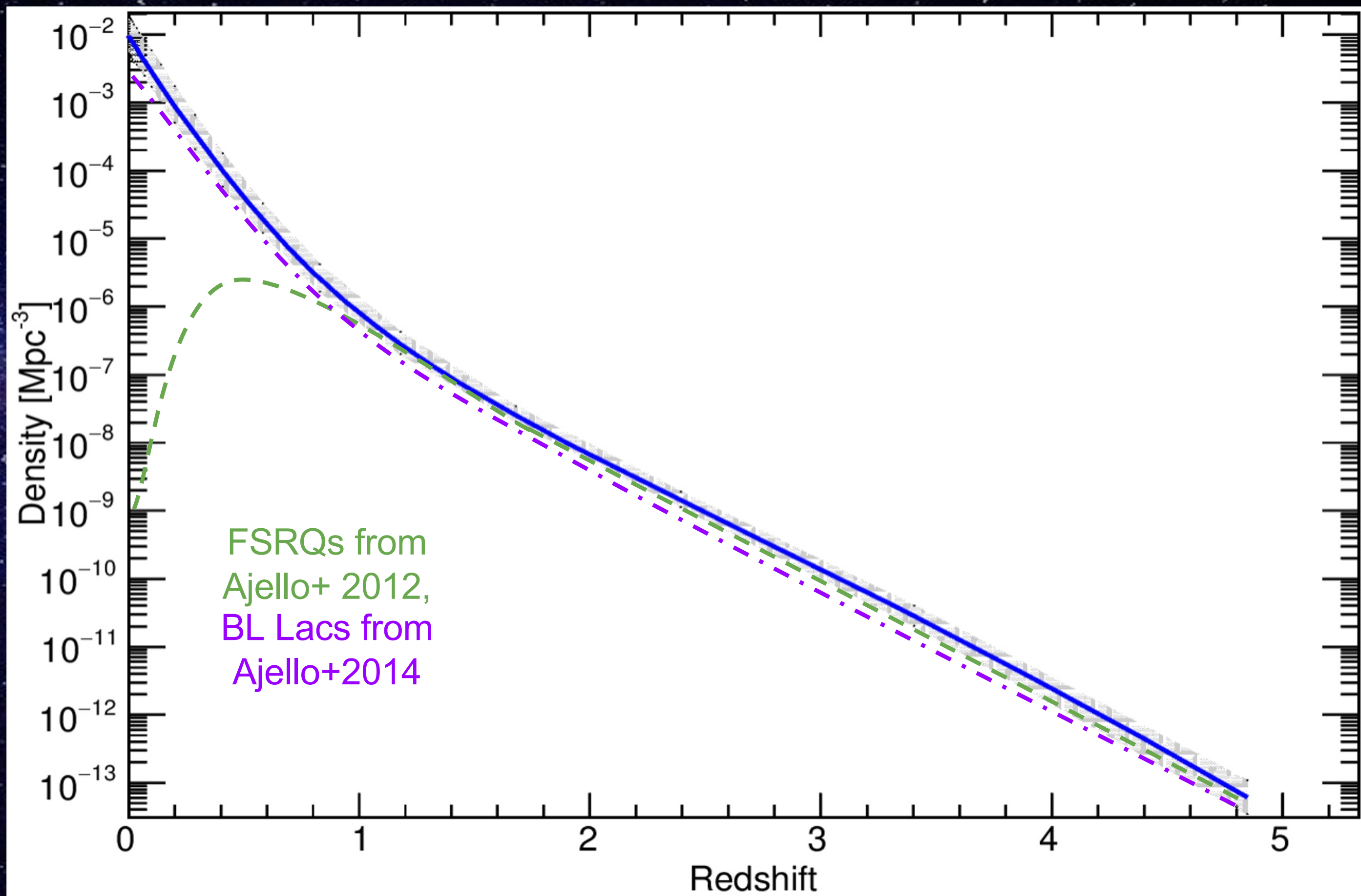

Cavaliere & D'Elia 2002
Böttcher & Dermer 2002

Luminosity Density of Blazars

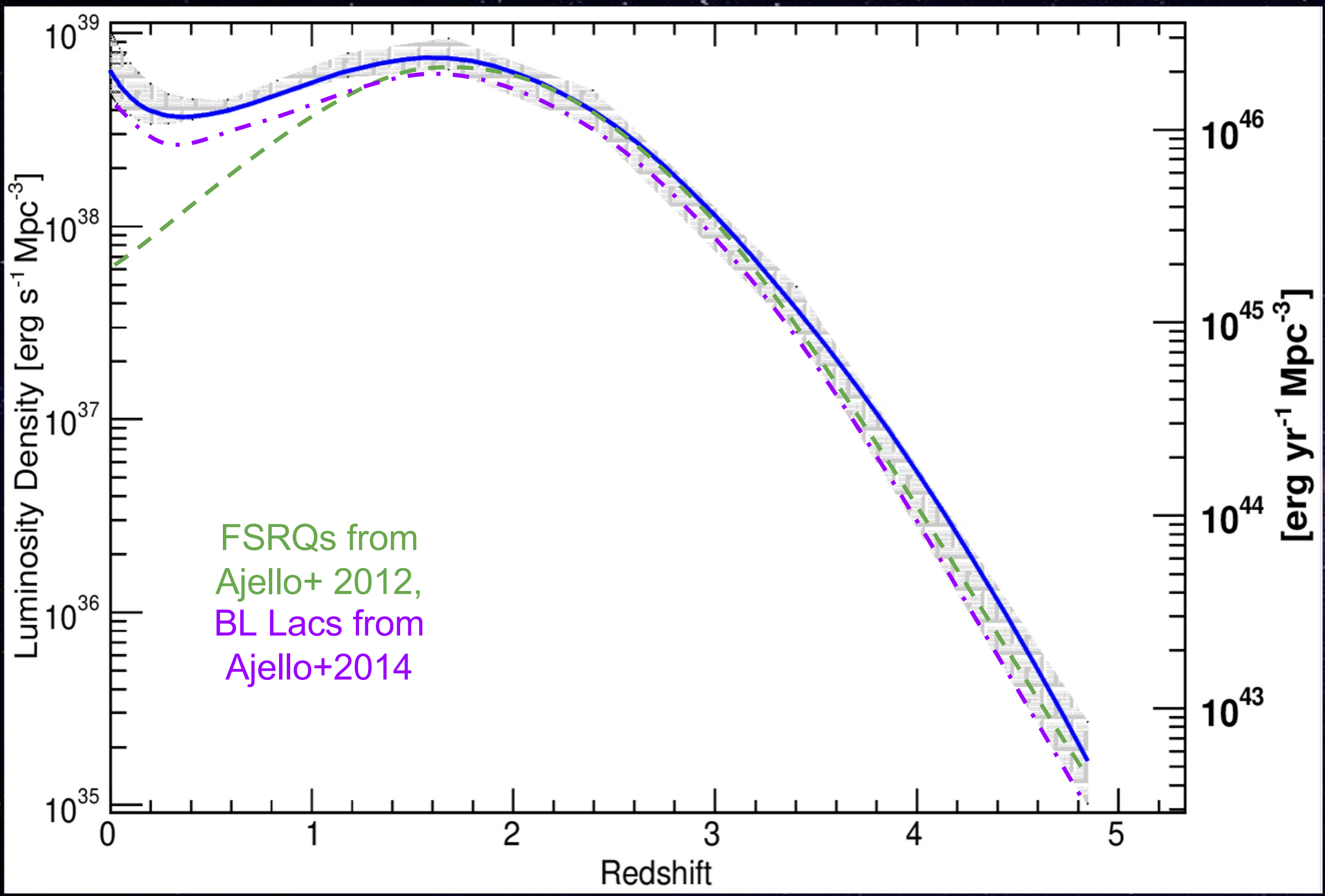

Hint towards different peaks of FSRQs and BL Lacs.

Conclusion

LF follows a double power-law shape.

LF extends to 4 orders of magnitude lower in luminosities than previous studies.

LF seems to be best represented by LDDE.

Hint of a link between FSRQs and BL Lacs can be seen.

Separate analysis of FSRQs and BL Lacs is required.

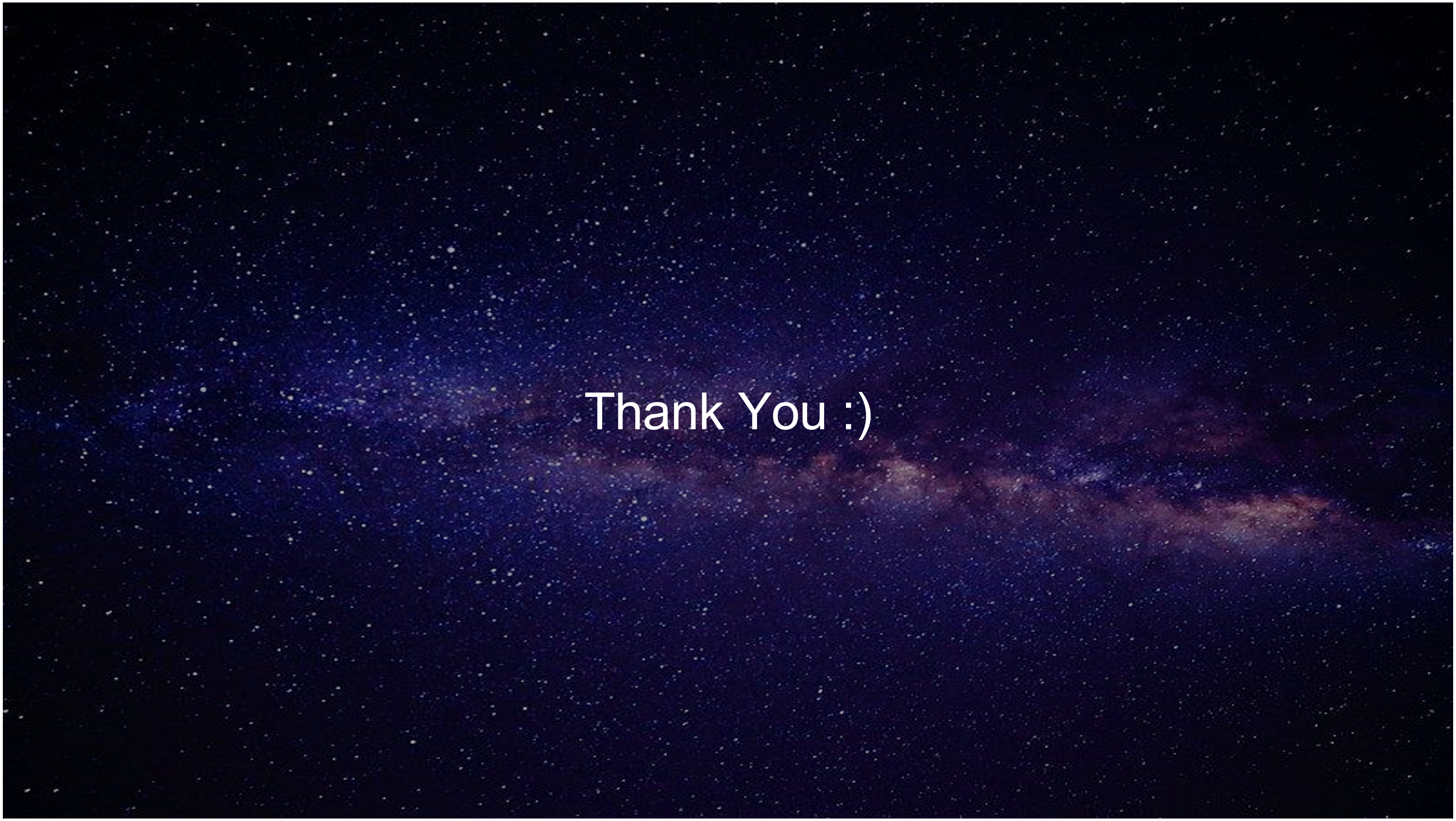
Thank You :)

Luminosity Histogram

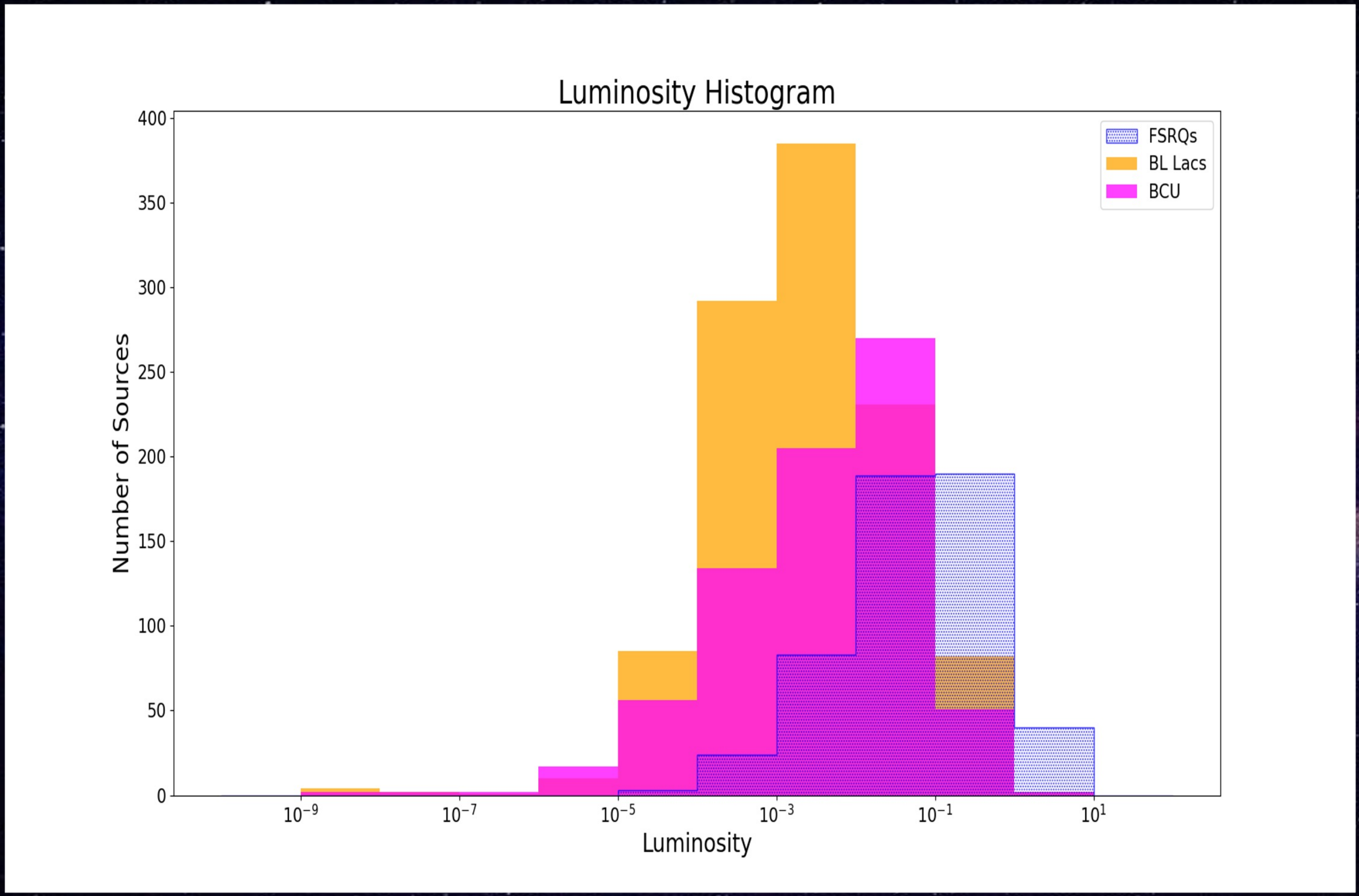

PDE Parameters

L_star = 1.630855e-03 * 1e48 = 1.63e45 erg/s

k = 15.98

\xi = -0.117

gamma1 = 1.23

gamma2 =2.05

\tau = 3.325

$$\Phi(L_\gamma, z=0, \Gamma) = \frac{A}{\ln(10) L_\gamma}\left[\left(\frac{L_\gamma}{L_*}\right)^{\gamma_1} + \left(\frac{L_\gamma}{L_*}\right)^{\gamma_2}\right]^{-1} \times e^{-\frac{(\Gamma-\mu(L_\gamma))^2}{2\sigma^2}},$$

$$e(z) = (1+z)^{k_d} e^{z/\xi},$$

Lum

z

$$k_d = k^* + \tau \times (\log_{10}(L_\gamma) - 46).$$

$$\Phi(L_\gamma, z, \Gamma) = \Phi(L_\gamma, z=0, \Gamma) \times e(z),$$

Methodology

Fit various LF models on the data (PLE, PDE, LDDE)

z_0 (=0) $<$ z_1 $<$ z_2

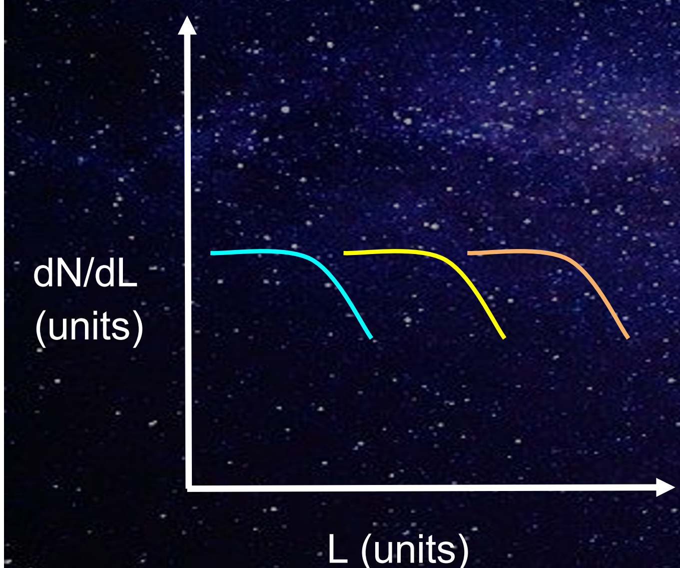

Pure Luminosity
Evolution (PLE)

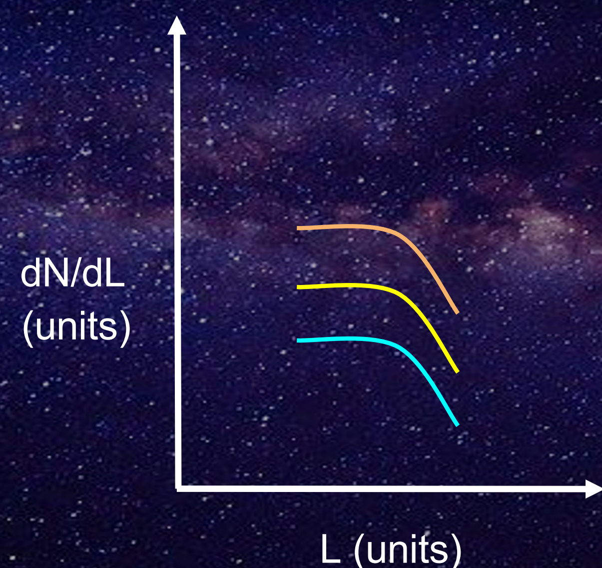

Pure Density
Evolution (PDE)

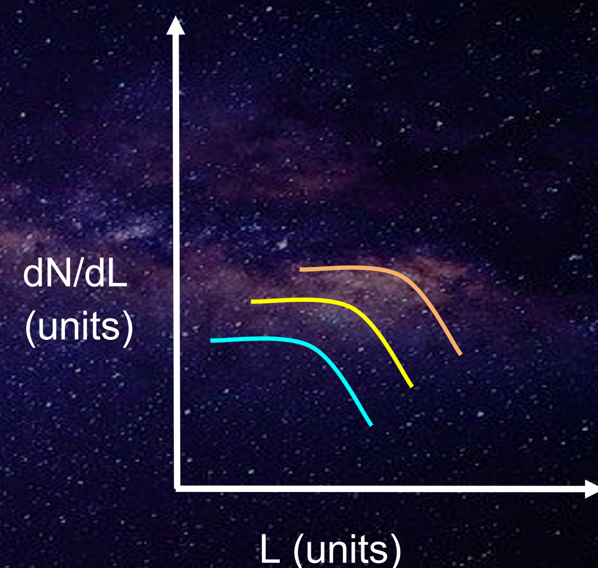

Luminosity-Dependent
Density Evolution (LDDE)

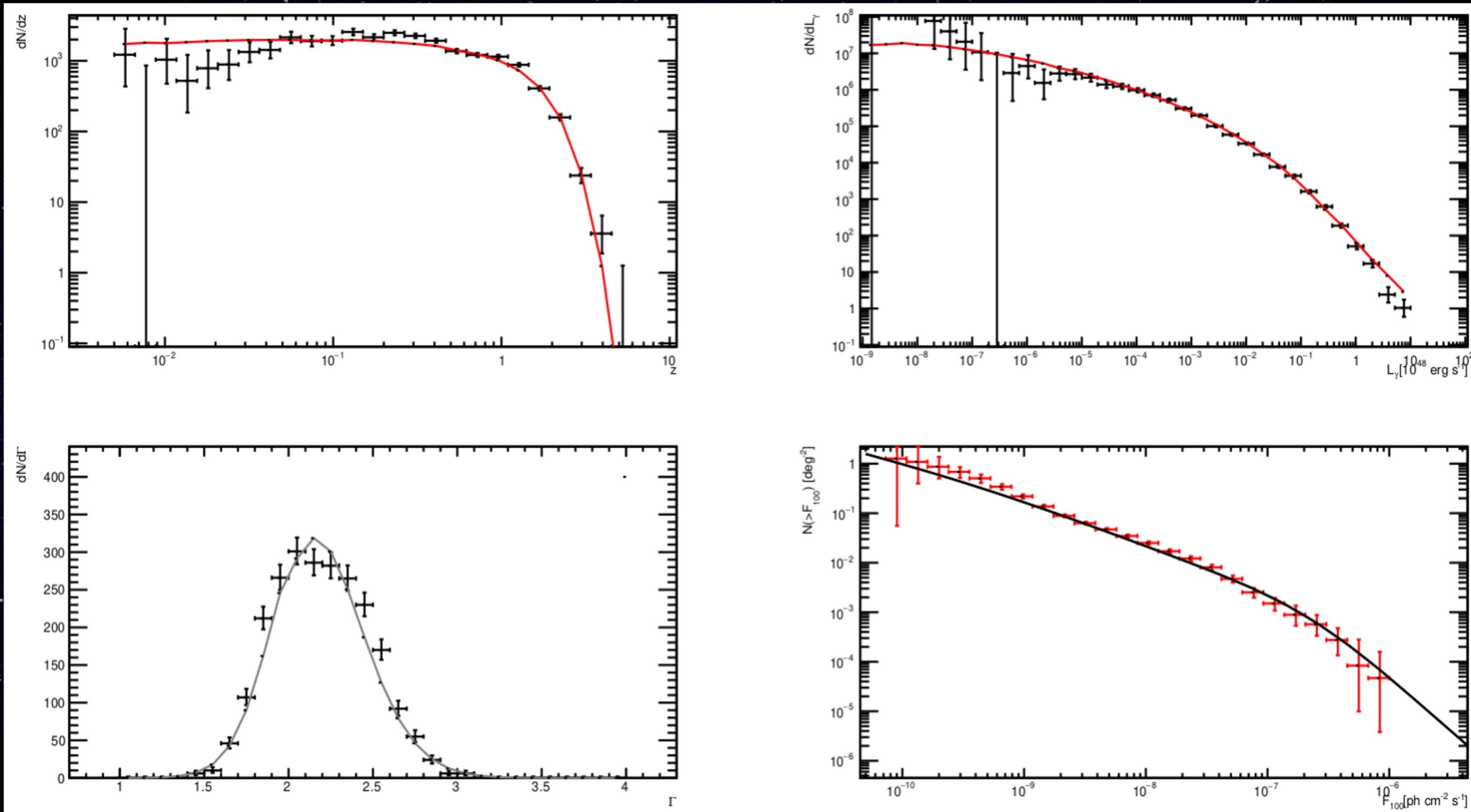

dN/dz
z
dN/dL$_\gamma$
L$_\gamma$[10^{48} erg s^{-1}]
dN/dΓ
Γ
N(>F$_{100}$) [deg^{-2}]
F$_{100}$[ph cm^{-2} s^{-1}]

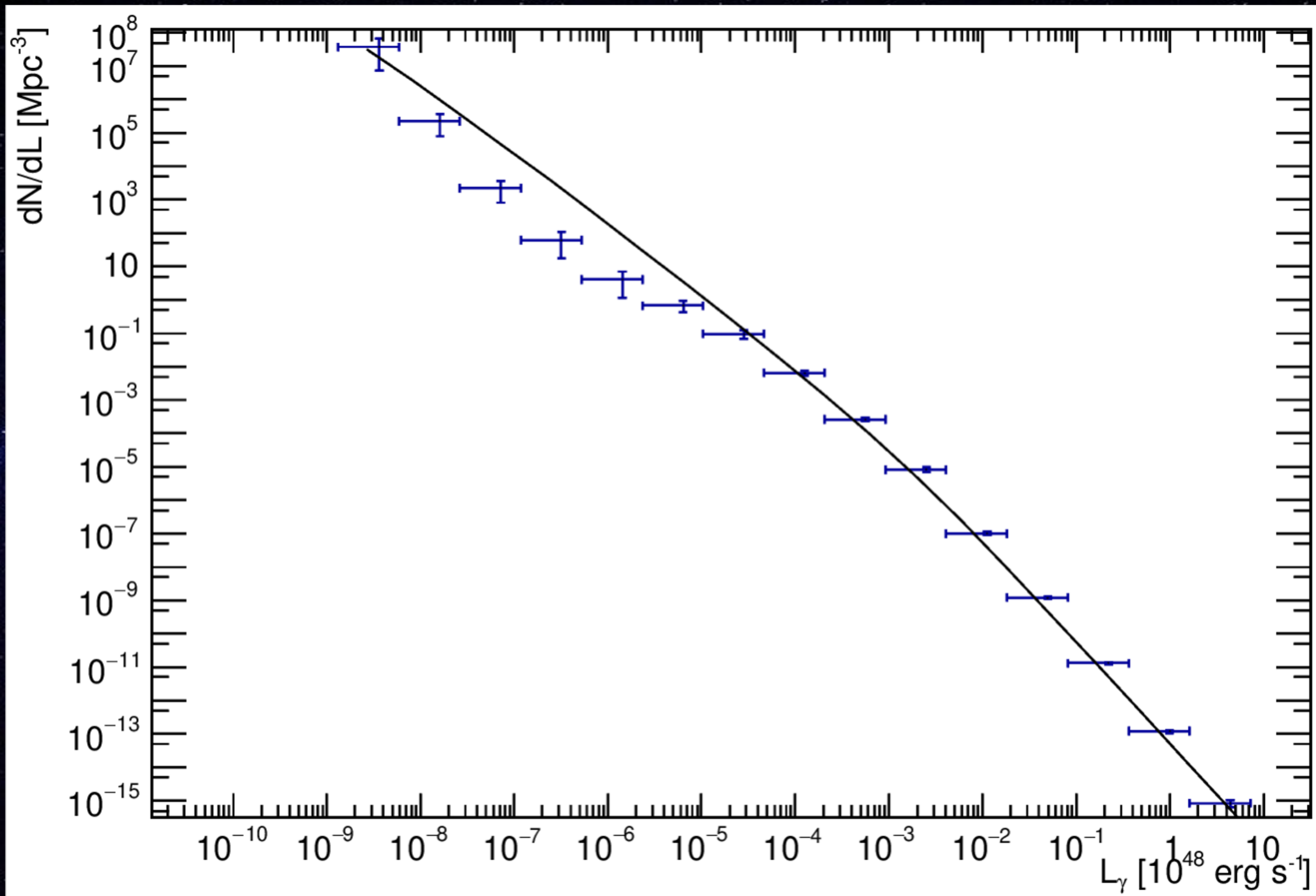

dN/dL [Mpc^{-3}]
10^{8}
10^{7}
10^{5}
10^{3}
10
10^{-1}
10^{-3}
10^{-5}
10^{-7}
10^{-9}
10^{-11}
10^{-13}
10^{-15}
10^{-10} 10^{-9} 10^{-8} 10^{-7} 10^{-6} 10^{-5} 10^{-4} 10^{-3} 10^{-2} 10^{-1} 1 10
L_γ [10^{48} erg s^{-1}]

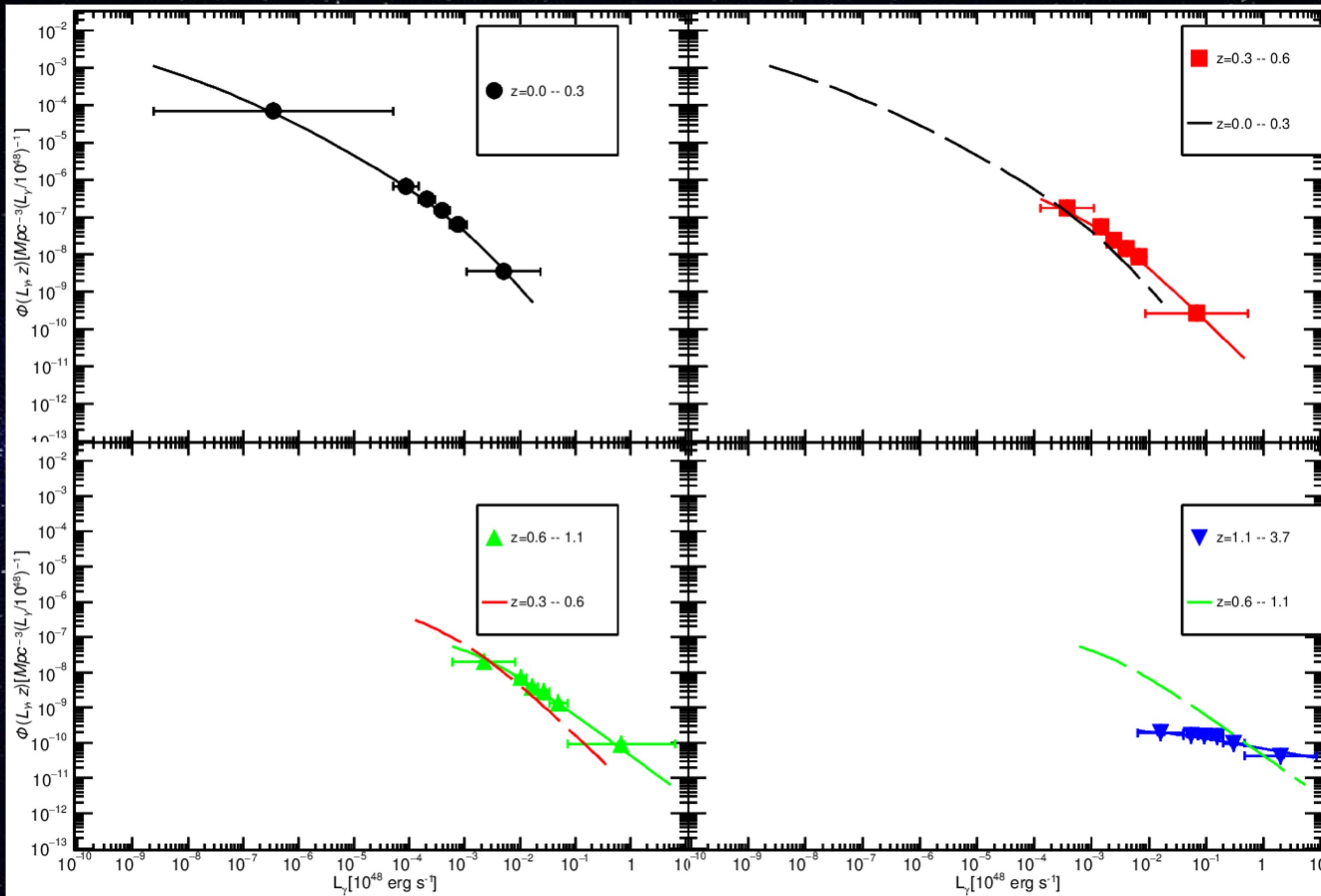
z=0.0 -- 0.3
z=0.3 -- 0.6
z=0.0 -- 0.3
z=0.6 -- 1.1
z=0.3 -- 0.6
z=1.1 -- 3.7
z=0.6 -- 1.1
$\Phi(L_\gamma, z)[Mpc^{-3}(L_\gamma/10^{48})^{-1}]$
$L_\gamma[10^{48}$ erg s$^{-1}]$

Luminosity Function (LF)

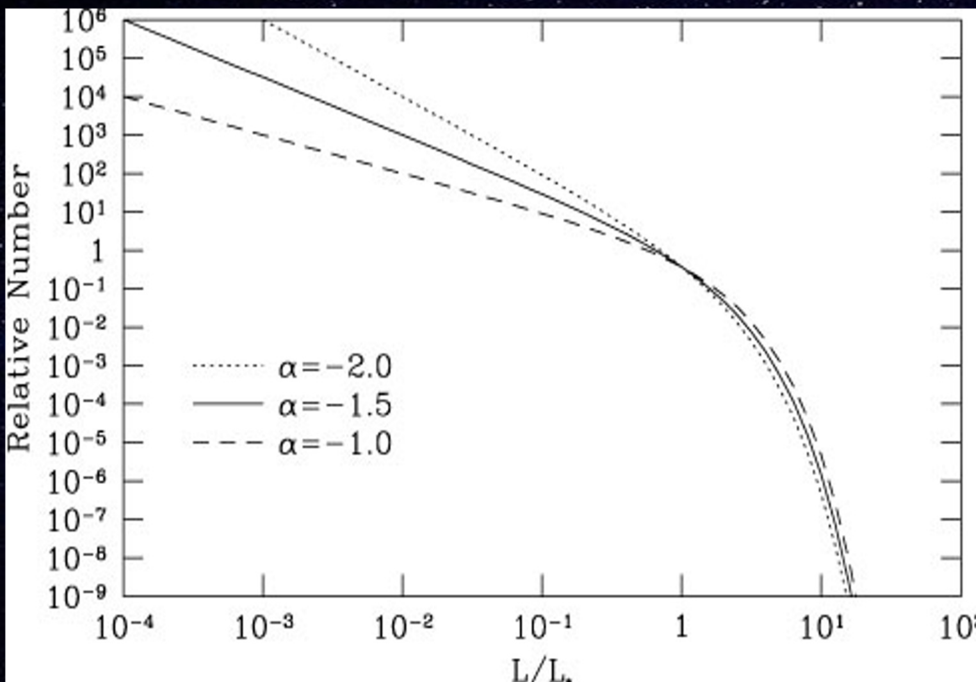

LF (ϕ) informs us on the number of objects per unit comoving volume and luminosity interval.

We can get other quantities of interest from LF:

Number density $$n = \int_L^\infty \Phi(L)dL$$

Luminosity density $$\int_L^\infty \Phi(L)LdL$$

https://jila.colorado.edu

Redshift of BLL

- Photometric dropout technique (Lower or Higher limit).
- Metal line absorption systems (Lower limit).
- Host Galaxy Spectral Fitting (Lower limit) - assuming M_R of elliptical galaxy to be same for all cases, host non-detection places lower limit on z.

Create PDF of *z* for each source. Compute LF using *z* from PDF. Use LF to predict observe *dN/dz*. Different? → replace with computed *dN/dz* and iterate to converge.

Redshift Distribution

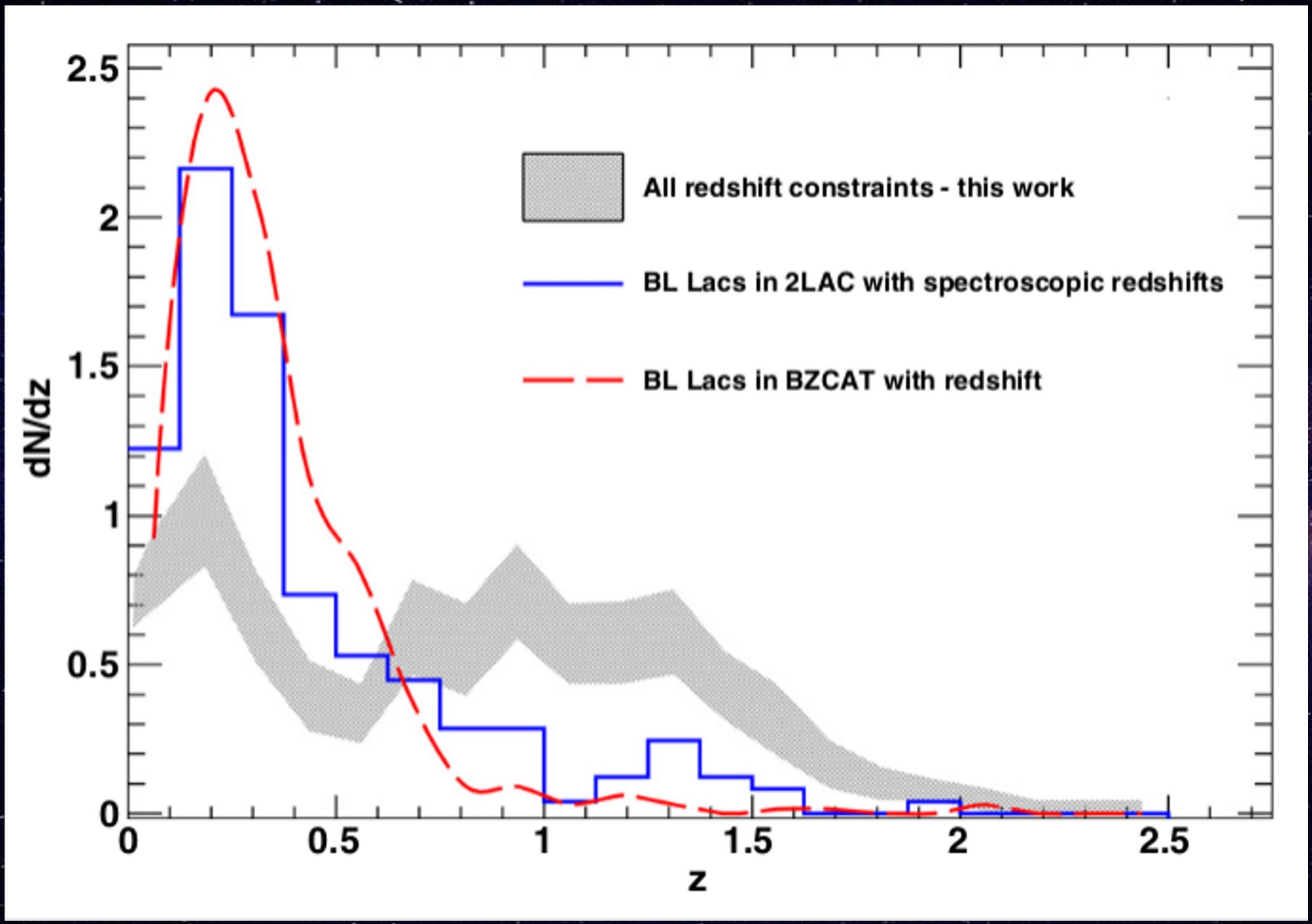

Method

Maximum-Likelihood (ML) Method used to derive LF (Φ).

Number density of BLL as function of *L, z* and ***Γ*** :

$$\frac{\partial^3 N}{\partial L_\gamma \partial z \partial \Gamma} = \frac{\partial^3 N}{\partial L_\gamma \partial V \partial \Gamma} \times \frac{dV}{dz} = \Phi(L_\gamma, V(z), \Gamma) \times \frac{dV}{dz},$$

The best-fit LF is found by comparing, through an ML estimator, the number of expected objects (for a given model LF) to the observed number while accounting for selection effects.

L-z plane parsed into tiny intervals *dLdz*. Expected number of blazars for each interval :

$$\lambda(L_\gamma, z, \Gamma) dL_\gamma dz d\Gamma = \Phi(L_\gamma, V(z), \Gamma) \cdot \Omega(L_\gamma, z, \Gamma) \times \frac{dV}{dz} dL_\gamma dz d\Gamma,$$

Intervals will contain either 0 or 1 BLL.

Maximum-Likelihood (ML) Method

We know that Poisson probability is: $$f(x) = \frac{\lambda^x}{x!} e^{-\lambda}$$, x = no. of successes.

For our case, x = 0 or 1.

The Likelihood function is given by the product of probabilities, such that for each *L-z* bin there is exactly 1 BLL and 0 otherwise:

$$L = \prod_i \lambda(L_{\gamma,i}, z_i, \Gamma_i)\, dL_\gamma\, dz\, d\Gamma\, e^{-\lambda(L_{\gamma,i}, z_i, \Gamma_i) dL_\gamma\, dz\, d\Gamma} \times \prod_j e^{-\lambda(L_{\gamma,j}, z_j, \Gamma_j) dL_\gamma\, dz\, d\Gamma}.$$

Function to minimize:

$$S = -2 \sum_i \ln \frac{\partial^3 N}{\partial L_\gamma \partial z \partial \Gamma} + 2 \int_{\Gamma_{min}}^{\Gamma_{max}} \int_{L_{\gamma,min}}^{L_{\gamma,max}} \times \int_{z_{min}}^{z_{max}} \lambda(L_\gamma, \Gamma, z)\, dL_\gamma\, dz\, d\Gamma.$$

Test of LF Model

Comparison of Data and Predictions:

$$\frac{dN}{dz} = \int_{\Gamma_{\min}}^{\Gamma_{\max}} \int_{L_{\gamma,\min}}^{L_{\gamma,\max}} \lambda(L_\gamma, \Gamma, z) dL_\gamma d\Gamma,$$

$$\frac{dN}{dL_\gamma} = \int_{\Gamma_{\min}}^{\Gamma_{\max}} \int_{z_{\min}}^{z_{\max}} \lambda(L_\gamma, \Gamma, z) dz d\Gamma,$$

$$\frac{dN}{d\Gamma} = \int_{L_{\gamma,\min}}^{L_{\gamma,\max}} \int_{z_{\min}}^{z_{\max}} \lambda(L_\gamma, \Gamma, z) dL_\gamma dz.$$

$$N(>F) = \int_{\Gamma_{\min}}^{\Gamma_{\max}} \int_{z_{\min}}^{z_{\max}} \int_{L_\gamma(z,F)}^{L_{\gamma,\max}} \Phi(L_\gamma, V(z), \Gamma) \frac{dV}{dz} d\Gamma dz dL_\gamma,$$

N^{obs}/N^{model} Method:

$$\Phi(L_{\gamma,i}, V(z_i), \Gamma_i) = \Phi^{\mathrm{mdl}}(L_{\gamma,i}, V(z_i), \Gamma_i) \frac{N_i^{\mathrm{obs}}}{N_i^{\mathrm{mdl}}},$$

LF Model

Photon Index → Gaussian distribution.

Local LF (DPL):

$$\Phi(L_\gamma, z=0, \Gamma) = \frac{A}{\ln(10) L_\gamma}\left[\left(\frac{L_\gamma}{L_*}\right)^{\gamma_1} + \left(\frac{L_\gamma}{L_*}\right)^{\gamma_2}\right]^{-1} \times e^{-\frac{(\Gamma-\mu(L_\gamma))^2}{2\sigma^2}},$$

Low luminosity - flatter, high lum - steeper slope.

Low lum objects are more common than high lum. Turnover luminosity is useful when comparing LFs for different *z* or *L*.

PLE & PDE:

$$e(z) = (1+z)^{k_d} e^{z/\xi},$$

Lum *z*

$$k_d = k^* + \tau \times (\log_{10}(L_\gamma) - 46).$$

For the PDE the evolution is defined as

$$\Phi(L_\gamma, z, \Gamma) = \Phi(L_\gamma, z=0, \Gamma) \times e(z), \quad (15)$$

while for the PLE case it is

$$\Phi(L_\gamma, z, \Gamma) = \Phi(L_\gamma / e(z), \Gamma). \quad (16)$$

The PLE and PDE models have 10 free parameters (A, γ_1, L_*, γ_2, k^*, τ, ξ, μ^*, β, and σ).

LDDE

$$\Phi(L_\gamma, z, \Gamma) = \Phi(L_\gamma, z = 0, \Gamma) \times e(z, L_\gamma), \tag{17}$$

where

$$e(z, L_\gamma) = \left[\left(\frac{1+z}{1+z_c(L_\gamma)} \right)^{p1(L_\gamma)} + \left(\frac{1+z}{1+z_c(L_\gamma)} \right)^{p2} \right]^{-1} \tag{18}$$

$$z_c(L_\gamma) = z_c^* \cdot (L_\gamma / 10^{48})^{\alpha}, \tag{19}$$

$$p1(L_\gamma) = p1^* + \tau \times (\mathrm{Log}_{10}(L_\gamma) - 46). \tag{20}$$

Methodology

Fit various LF models on the data (PLE, PDE, LDDE).

Local Luminosity Function (z=0):

$$\phi(L_\gamma, z=0) = \frac{dN}{dL_\gamma dV} = \frac{A}{ln(10)L_\gamma}\left[\left(\frac{dL_\gamma}{dL_*}\right)^{\gamma_1} + \left(\frac{dL_\gamma}{dL_*}\right)^{\gamma_2}\right]^{-1}$$

Including Evolution (z dependence), e.g. PDE:

$$\Phi(L_\gamma, z) \quad = \quad \Phi(L_\gamma, z=0) \times e(z, L_\gamma)$$

Evolutionary Term:

$$e(z, L_\gamma) = (1+z)^{k_d} e^{z/\xi}$$

$$k_d = k^* + \tau \times [log(L_\gamma) - 46]$$

The V/V_max Test

$$\left\langle \frac{V}{V_{\max}} \right\rangle = \frac{1}{n} \cdot \sum_{i=1}^{n} \frac{V_i}{V_{\max}}$$

Value within [0,1]

Value= 0.5 → equally distributed. Value>0.5 → positive evolution.

Would introduce bias if there is evolution within *z* bins.

$$V_{\mathrm{MAX}} = \int_{z_{\min}}^{z_{\max}} \Omega(L_i, z, \Gamma) \frac{e(z, L_i)}{e(z_{\min}, L_i)} \frac{dV}{dz} dz,$$

Comoving Volume

Hogg 1999

Dashed line

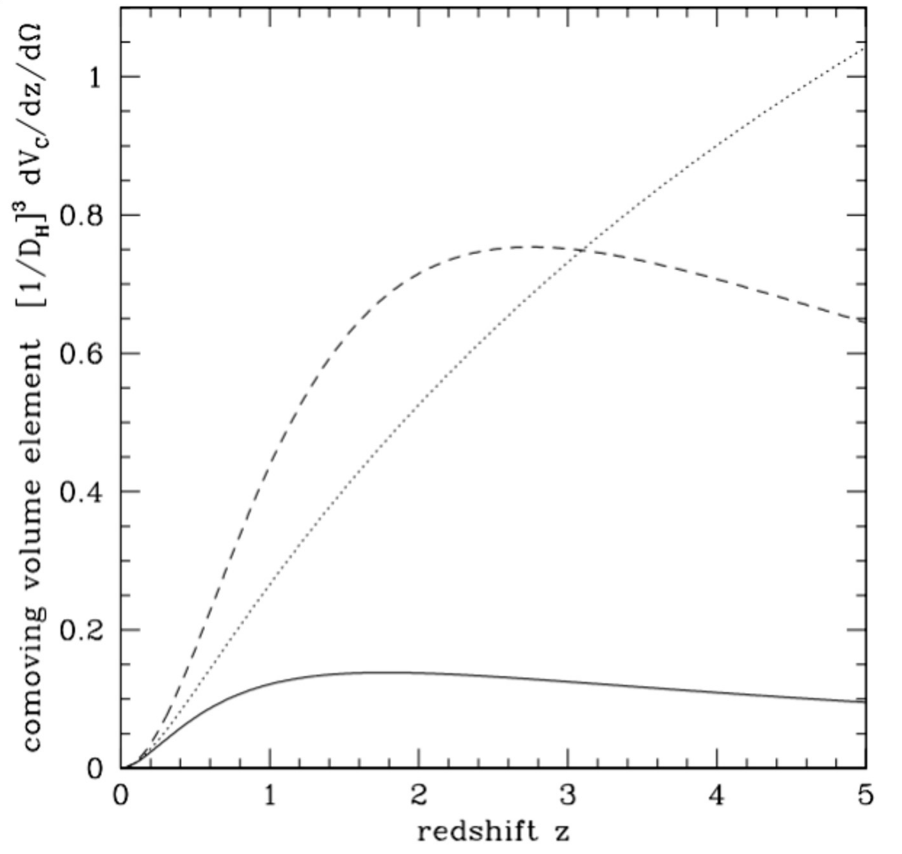

Figure 5: The dimensionless comoving volume element $(1/D_H)^3\,(dV_C/dz)$. The three curves are for the three world models, $(\Omega_M, \Omega_\Lambda) = (1, 0)$, solid; $(0.05, 0)$, dotted; and $(0.2, 0.8)$, dashed.

Algorithm

- ❑ Prior function for *dN/dz.*
- ❑ Simulate 1000 samples, with z from PDF.
- ❑ Use ML to derive best-fit LF for each sample. Final LF → average of 1000 LF.

  This enables us to derive the uncertainty as well.

- ❑ Compare *dN/dz*, if different: use latest *dN/dz*. Repeat till both match.

BLL, FSRQ, BCU

Optical classification - different resources, in decreasing order of precedence: **optical spectra** from our intensive follow-up program (Shaw et al. 2013), the BZCAT list (i.e., classification from this list, which is a compilation of sources ever classified as blazars, Massaro et al. 2009), and **spectra available in the literature**, e.g., SDSS (Ahn et al. 2012), 6dF (Jones et al. 2009).

The ***BCU*—blazar candidates of uncertain type** , from BZCAT/ radio data/ double-humped SED. BCUs are divided into three sub-types:

BCU I: the counterpart has a published optical spectrum but is not sensitive enough for a classification as an FSRQ or a BL Lac;

BCU II: the counterpart is lacking an optical spectrum but a reliable evaluation of the SED synchrotron-peak position is possible;

BCU III: the counterpart is lacking both an optical spectrum and an estimated synchrotron-peak position but shows blazar-like broadband emission and a flat radio spectrum;

3LAC: 10.1088/0004-637X/810/1/14

Fermi LAT Biases

1. Spectral bias (or photon-index bias). It is the selection effect which allows Fermi-LAT to detect spectrally hard sources at fluxes generally fainter than those of soft sources.

2. Malmquist bias: in a brightness-limited survey, where stars below a certain apparent brightness cannot be included. Since observed stars and galaxies appear dimmer when farther away, the brightness that is measured will fall off with distance until their brightness falls below the observational threshold.

3. Eddington bias: The flux (F) from astrophysical sources has a fluctuation of ΔF . If a source falls closely to the detection threshold of the instrument, it would be more easily detected if $F = F + \Delta F$. Therefore, such objects (~3% of the sample) are found with a higher flux than their intrinsic one.

Detection Efficiency (ω)

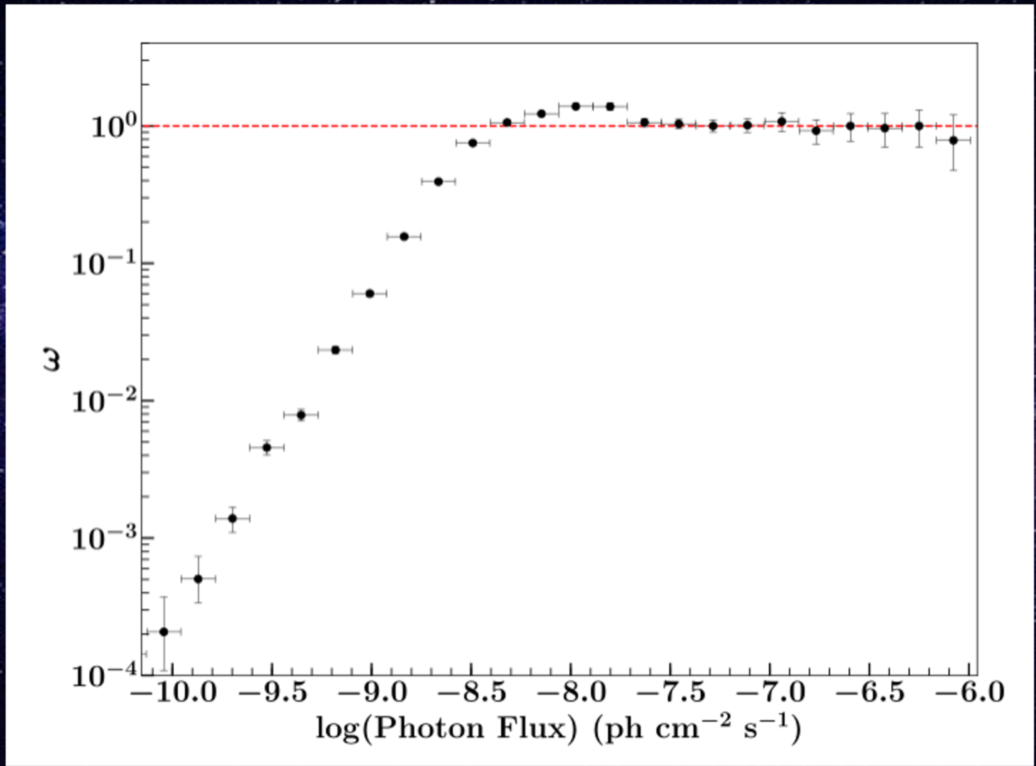

Marcotulli et al., 2020.

Efficiency Correction Method

Algorithm:

1) Point sources from LAT data - Real catalog.
2) Monte Carlo simulations to generate isotropic blazar distribution.

   Inputs → spectral and flux parameters from real blazars.

1) Detect point sources from simulated sky.
2) Derive detection efficiency (*ω(S)*).
3) Using *ω(S)* to correct the real catalog → account for biases.
4) Derive the intrinsic source count distribution (*logN-logS*).

Efficiency Correction Method

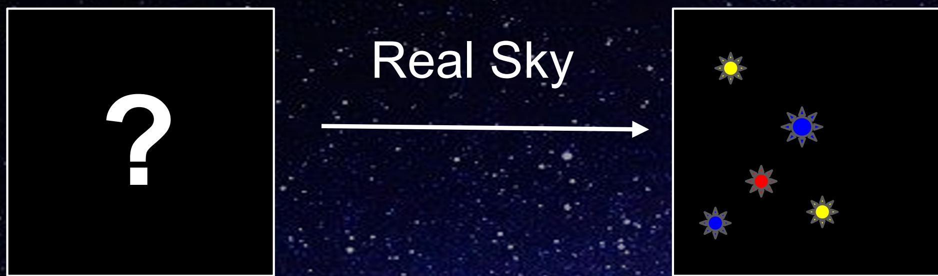

Intrinsic real sky not known. Running detection pipeline for observed real sky.

Simulating real sky and passing it through the detection pipeline to obtain detection efficiency.

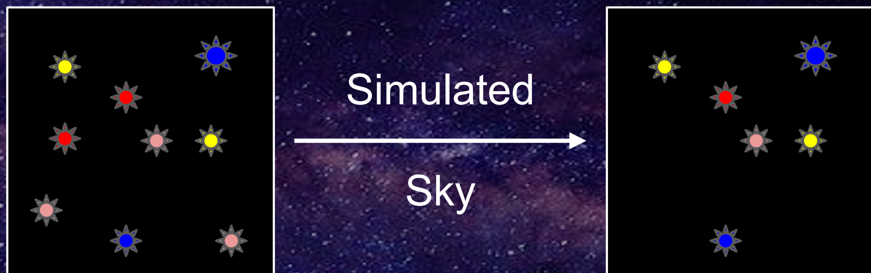

Using the detection efficiency to obtain the intrinsic real sky.

= Bright = Faint

Monte Carlo Simulations

To use randomness to solve problems that might be deterministic in principle.

Monte Carlo methods vary, but tend to follow a particular pattern:

1. Define a domain of possible inputs
2. Generate inputs randomly from a probability distribution over the domain
3. Perform a deterministic computation on the inputs
4. Aggregate the results

Markov Chains: At the core of MCMC is the concept of Markov chains. A Markov chain is a process where the probability of transitioning from one state to another depends only on the current state, not on the sequence of states that preceded it. In simpler terms, it's a random process where the future state depends only on the present state, not on the past.
One of the critical aspects of MCMC methods is ensuring convergence, meaning that the sequence of sampled states eventually settles into the true distribution.

Diffused EGB

There are two possibilities for the origin of the diffused extragalactic EGB:

(1) it is truly diffuse; and

(2) it is the integrated emission of various distant unresolved gamma-ray sources.

It may also be a combination of diffuse and point sources and may have different origins in different portions of the gamma-ray band. From below 10 MeV to 100 MeV, particle-antiparticle annihilation, bremsstrahlung and inverse Compton interactions between cosmic ray particles and lower-energy photons are the most likely gamma-ray production mechanisms.

Above 100 MeV, the dominant process is decay from nucleon interactions. E.g. A cosmic-ray proton strikes another proton. The protons survive the collision, but their interaction creates an unstable particle — a pion — with only 14 percent the mass of a proton. In 10 millionths of a billionth of a second, the pion decays into a pair of gamma-ray photons.

Diffused process also include Dark matter annihilation.

Blazars contribute to the unresolved isotropic diffused EGB.

NED

Extragalactic Gamma-ray Background

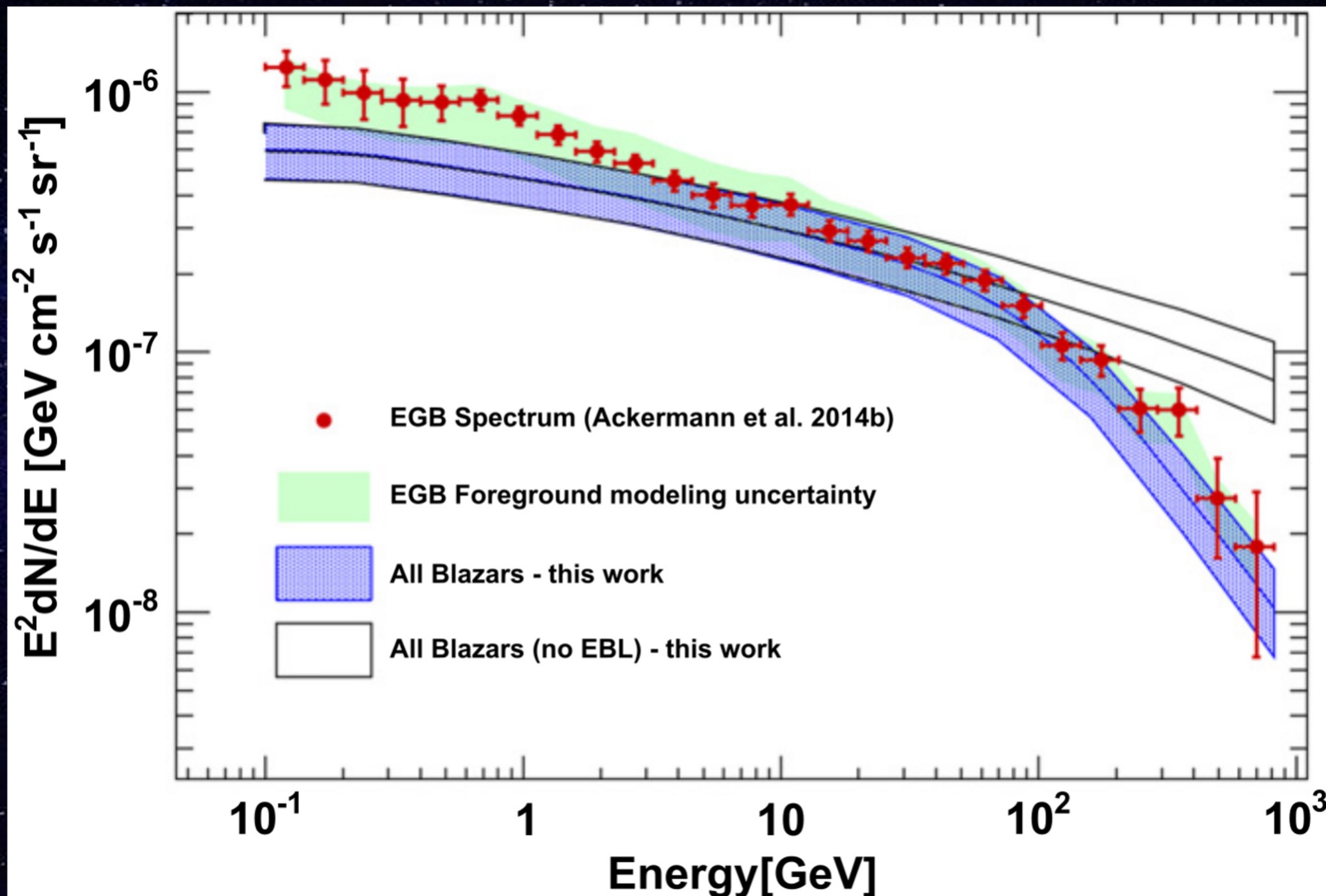

Discussions and Conclusions

- Contribution to EGB.

$$F_{EGB}(E_\gamma) = \int_{\Gamma_{min}=1.0}^{\Gamma_{max}=3.5} d\Gamma \int_{z_{min}=10^{-3}}^{z_{max}=6} dz \times \int_{L_\gamma^{min}=10^{[illegible]}}^{L_\gamma^{max}=10^{[illegible]}} dL_\gamma \cdot \Phi(L_\gamma, z, \Gamma) \cdot \frac{dN_\gamma}{dE} \cdot \frac{dV}{dz} \times (\mathrm{ph\ cm^{-2}\ s^{-1}\ sr^{-1}\ GeV^{-1}}),$$

Correcting the Real Sky

$$\frac{dN}{dS} = \frac{1}{\Omega \Delta S_i} \frac{N_i}{\omega(S_i)},$$

For efficiency < 1, in the denominator, there is an increase in the number. This accounts for low flux sources that were missed out in the uniform survey.

EGB

Total blazer contribution to EGB = 50 %. 27% of this 50% from unresolved sources.

Resolved sources

Unresolved sources

$$S_{\mathrm{EGB}} = \Sigma_{i=1}^{N} \frac{S_{\mathrm{PS},i}}{\Omega} + \int_{S_{\min}}^{S_{\max}} (1 - \omega(S'))S' \frac{dN}{dS'} dS'$$

Importance of Redshift Constraints

Using only spectroscopic *z* introduces bias in the *dN/dz*, and therefore the LF computed utilizing it.

More BLL at lower z.

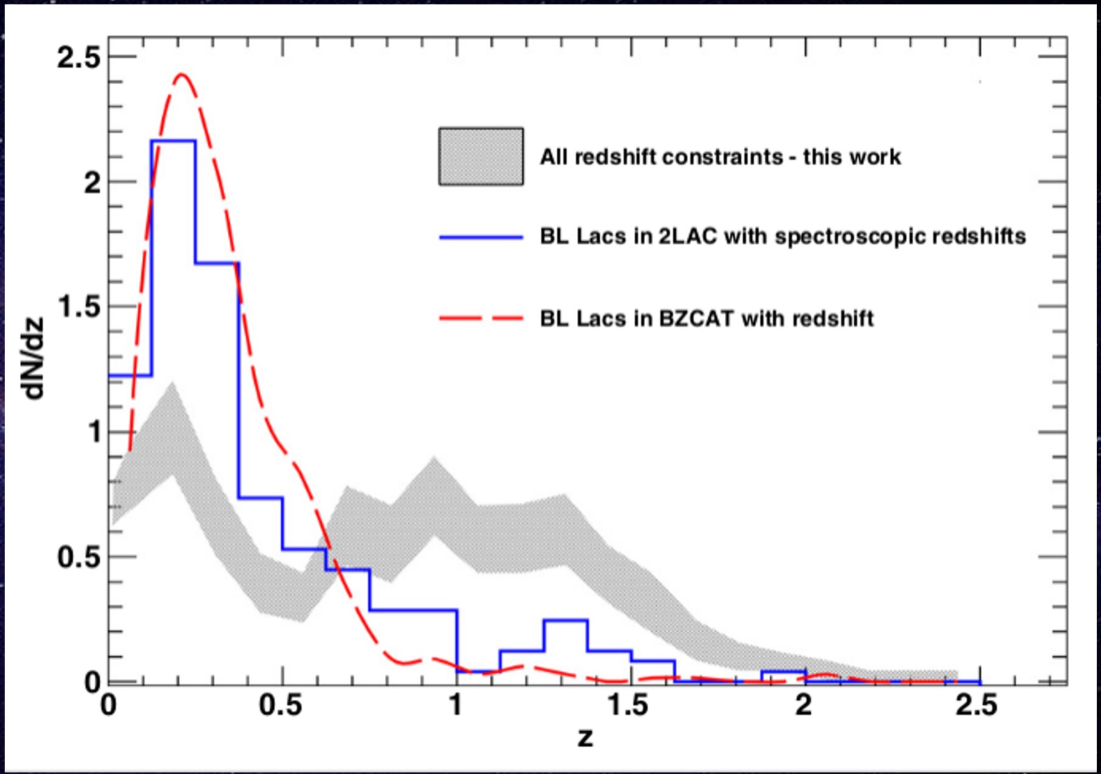

Electromagnetic Spectrum

1eV→10^4K

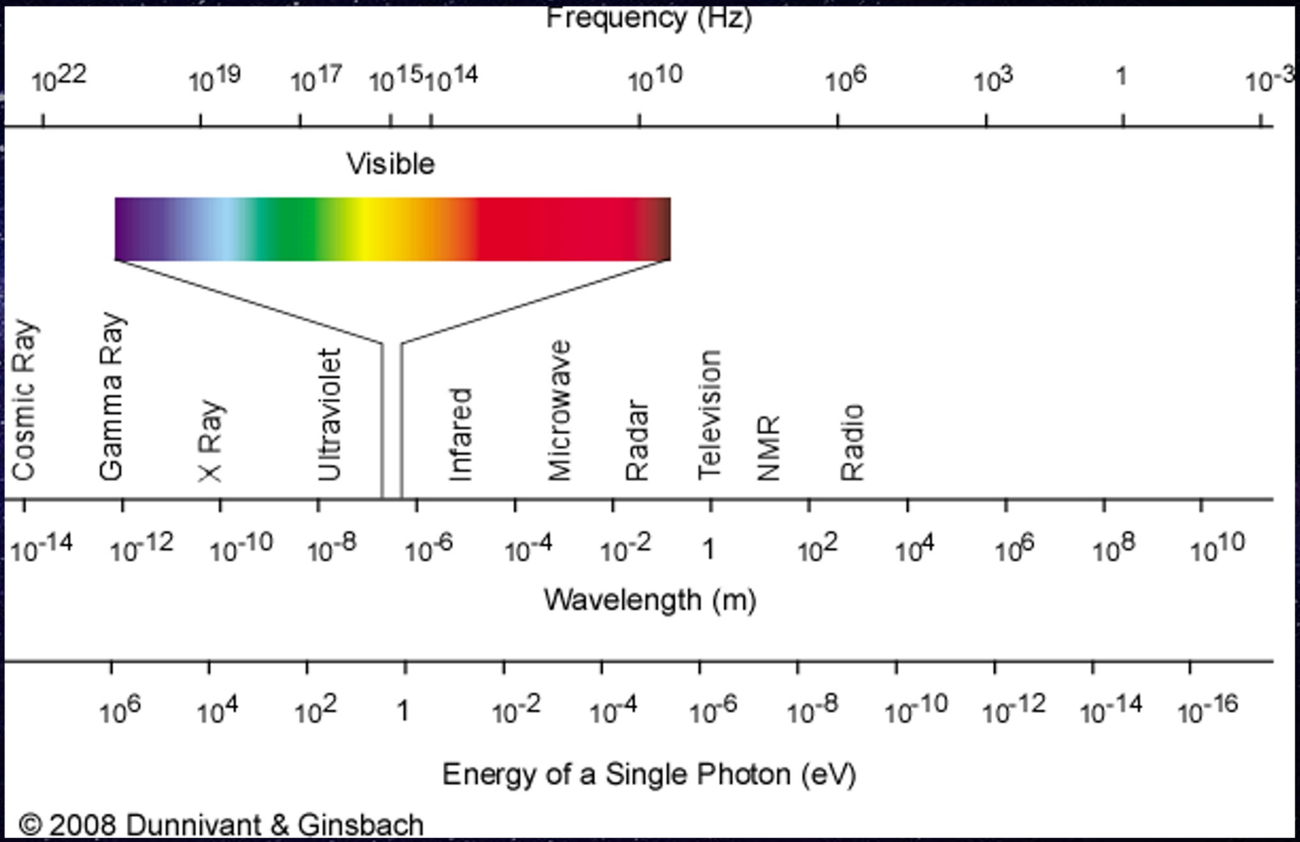

Blazar Model

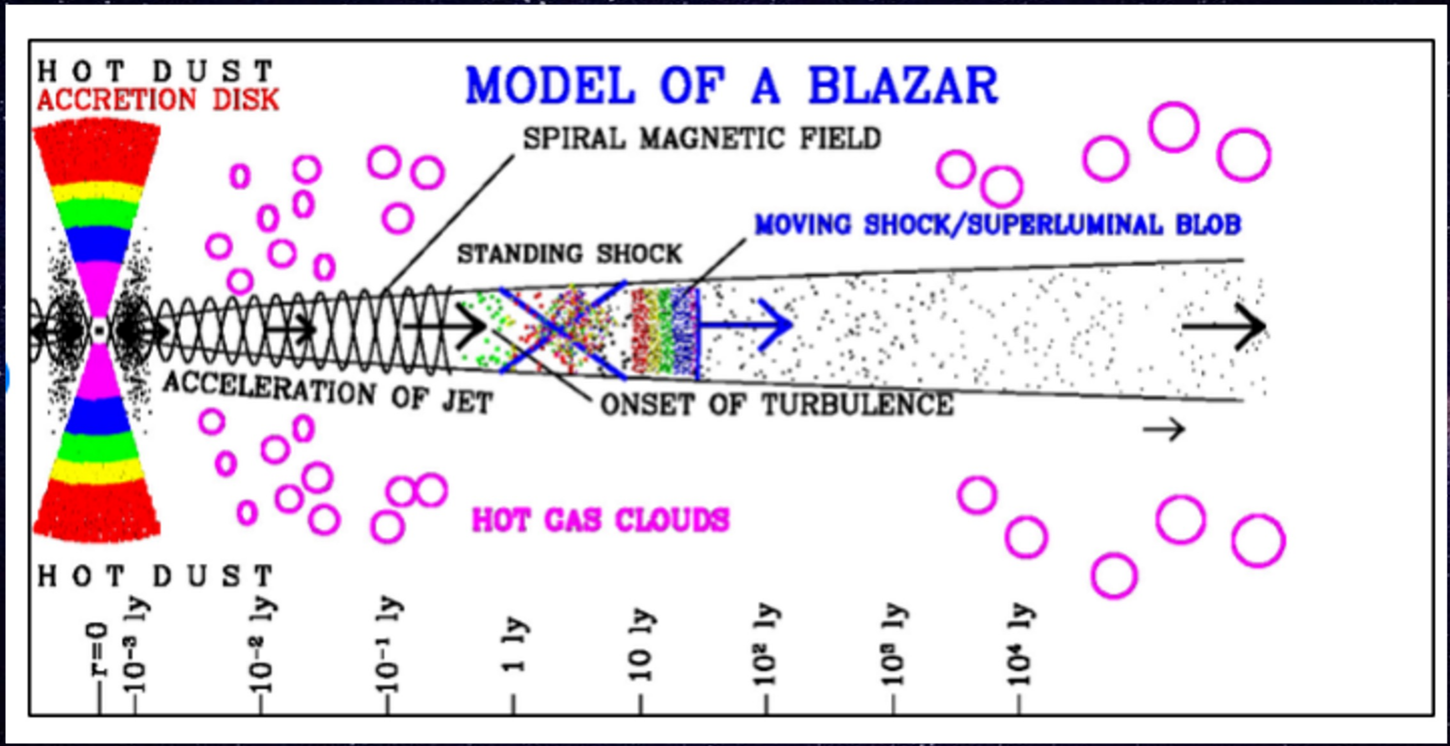

Park et al 2022

Synchrotron Emission + Beaming

$$\vec{E}_{rad} = \frac{q}{Rc^2}\left\{\vec{n}\times(\vec{n}\times\dot{\vec{u}})\right\}$$

$$|\vec{E}_{rad}| = \frac{q\dot{u}}{Rc^2}\sin\Theta$$

$$S = \frac{c}{4\pi}E_{rad}^2 = \frac{c}{4\pi}\frac{q^2\dot{u}^2}{R^2c^4}\sin^2\Theta$$

$$P = \frac{dW}{dt} = \frac{q^2\dot{v}^2}{4\pi c^3}\int\sin^2\Theta\, d\Omega$$

$$= \frac{2q^2\dot{u}^2}{3c^3}$$

$$a_\perp = \omega_B v_\perp = \frac{q}{\gamma mc}\vec{v}_\perp\times\vec{B}$$

$$\Rightarrow \omega_B = \frac{qB}{\gamma mc}$$

$$P = \frac{2q^2}{3c^3}\gamma^4(a_\perp^2+\gamma^2 a_\parallel^2)$$

$$L = P = \frac{4}{3}\sigma_T c\beta^2\gamma^2 U_B$$

$$N(E)\,dE = CE^{-p}\,dE$$

$$P \propto \omega^{-\alpha}$$

$$\alpha = \frac{p-1}{2}$$

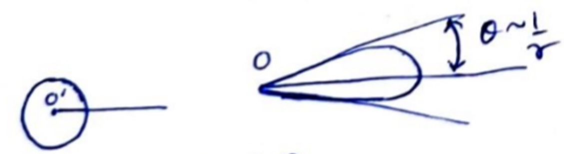

$$\tan\theta = \frac{u'\sin\theta}{\gamma(u'\cos\theta'+v)}$$

$$u' = c\,,\quad \theta = 90^\circ$$

$$\tan\theta = \frac{c}{\gamma v}$$

$$\theta\sim\frac{1}{\gamma}$$

Accretion Disk

Turbulent motions in the disk generate stresses that transport angular momentum outward.

The alpha-disk model provides a convenient way to parameterize the effects of turbulence.

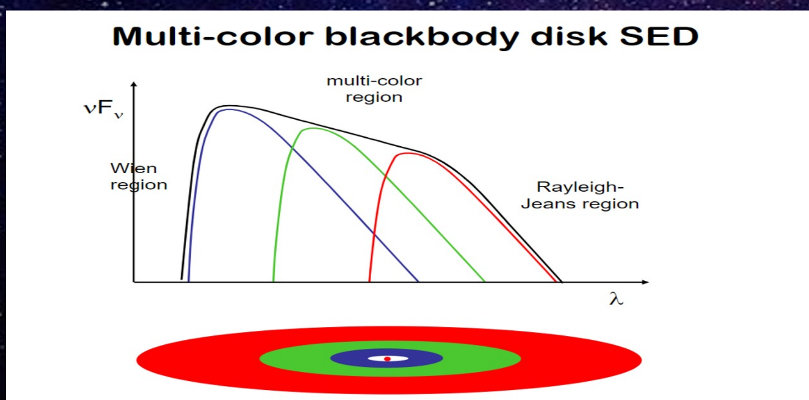

$$T \propto r^{-3/4}$$

$$\therefore L = \frac{GM\dot{M}}{2r} = 2\pi r^2 \sigma T^4$$

$$T \propto (M\dot{M})^{1/4} r^{-3/4}$$

$$\nu = \alpha c_s h$$

viscosity

$$T = \left[\frac{3GM\dot{M}}{8\pi\sigma r^3}\left(1 - \sqrt{\frac{R_{in}}{r}}\right)\right]^{1/4}$$

$$B_\nu = \frac{2h\nu^3}{c^2} \frac{1}{e^{h\nu/kT} - 1}$$

•

$$k = n\frac{2\pi}{L} \Rightarrow dn_x = \frac{k_x L_x}{2\pi}$$

$$dN = 2 \times \frac{V\,d^3k}{(2\pi)^3} \quad (3D)$$

$$c = \nu\lambda \Rightarrow dk = \frac{2\pi d\nu}{c}$$

$$dN = \frac{2V}{c^3} \nu^2 d\nu\, d\Omega$$

$$u_\nu = \frac{h\nu}{e^{\beta h\nu} - 1} \cdot \frac{2\nu^2}{c^3}$$

$$u_\nu = \frac{I_\nu}{c} = \frac{B_\nu}{c}$$

Inverse Compton Scattering

$$\Delta\lambda = \frac{h}{mc}(1-\cos\theta)$$

$$\epsilon_f = \frac{\epsilon_i}{1+\frac{\epsilon_i}{mc^2}(1-\cos\theta)}$$

$$\gamma h\nu \ll m_e c^2$$

$$h\tilde{\nu} = \gamma^2 h\nu$$

$$L \propto \gamma^2 U_{ph}$$
$$= \frac{4}{3}\sigma_T c \gamma^2 \beta^2 U_{ph}$$

Relativistic Doppler Effect

$$\vec{U} = \begin{bmatrix} \gamma c \\ \gamma v \\ 0 \\ 0 \end{bmatrix} \qquad \vec{P} = \begin{bmatrix} h\nu/c \\ (h\nu/c)\cos\theta \\ (h\nu/c)\sin\theta \\ 0 \end{bmatrix}$$

$$E = E' = \vec{P} \cdot \vec{U}$$

$$= \gamma h\nu - \gamma h\nu \beta \cos\theta$$

$$= \gamma h\nu (1 - \beta\cos\theta)$$

$$\nu' = \gamma\nu(1 - \beta\cos\theta)$$

$$= \delta\nu$$

$$\frac{I_\nu}{\nu^3} \rightarrow L.I.$$

BH Mass

$$R_s = \frac{2GM_{BH}}{c^2}$$

For $M_{BH} = 10^9 M_\odot$

$$R_s = 2.96 \times 10^{14} \text{ cm}$$

$$\simeq 0.0001 \text{ pc}$$

$$\frac{dP}{dr} = -\frac{GM\rho}{r^2} = -\frac{\sigma_T}{m_p} \cdot \rho \frac{L}{4\pi r^2 c}$$

$$\Rightarrow L_{EDD} = \left(\frac{\sigma_T}{m_p}\right)^{-1} 4\pi GMc$$

$$\simeq 1.3 \times 10^{38} \frac{M}{M_\odot} \text{ erg/s}$$

Mass of BH:

1) $M-\sigma$ Relation

2) Reverberation Mapping.

3) Calibration Curves

• BLR Velocity →	Fit Line Profile →	v(FWHM)
• BLR Radius →	Time Lag →	cτ
• BH Mass →	Using v and r →	$M \approx \frac{rv^2}{G}$;

Absorption + Doppler Broadening

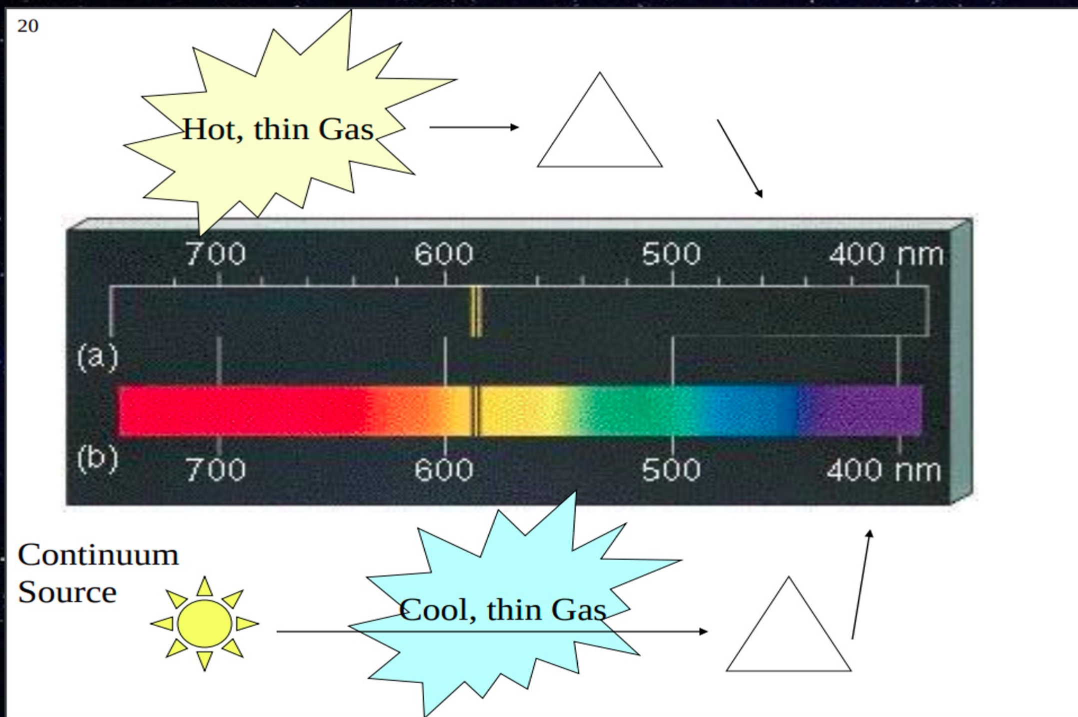

$$\tau_\nu(s) = \int_{s_0}^{s} \alpha_\nu(s')\, ds'$$

$$I_\nu(\tau_\nu) = I_\nu(0) e^{-\tau_\nu} + \int_0^{\tau_\nu} e^{-(\tau_\nu - \tau_\nu')} S_\nu(\tau_\nu')\, d\tau_\nu'$$

$$\frac{\nu - \nu_0}{\nu_0} = \frac{v_z}{c}$$

$$\phi(\nu) = \frac{1}{\Delta\nu_D \sqrt{\pi}} e^{-(\nu-\nu_0)^2/\Delta\nu_D^2}$$

$$\Delta\nu_D = \frac{\nu_0}{c}\sqrt{\frac{2kT}{m}}$$

Superluminal Motion in Jets

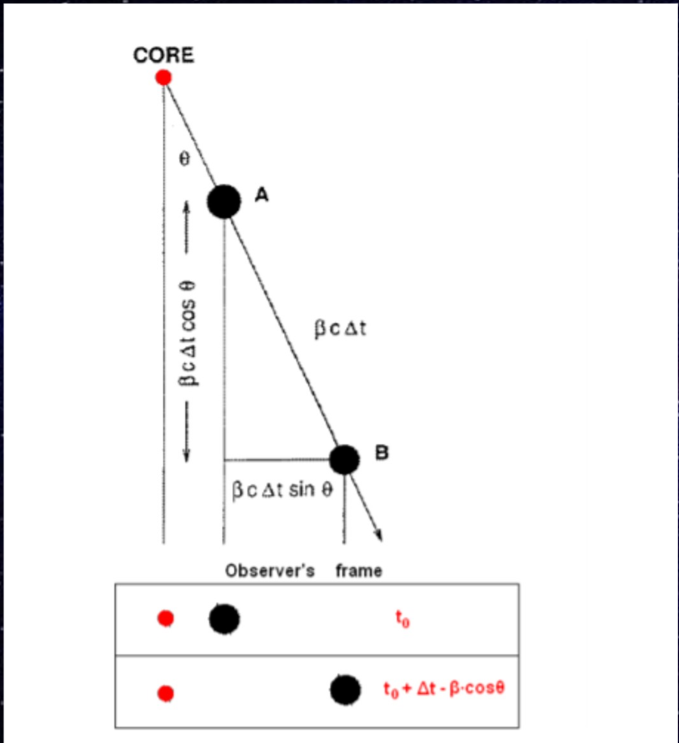

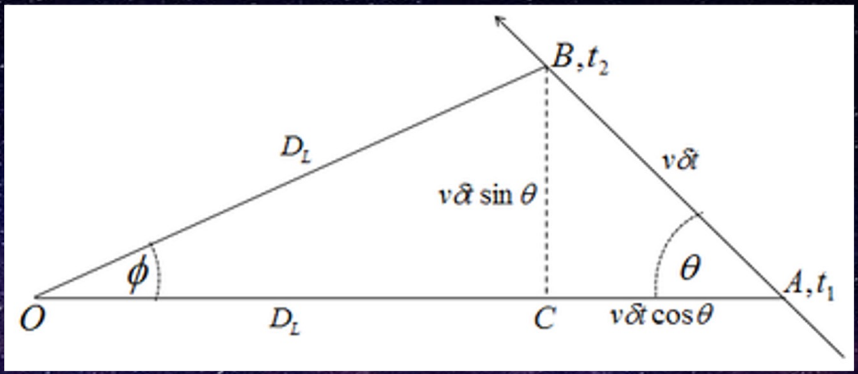

Dataset

2497 Sources from LAT 8-year Source List (Marcotulli 2020).

100 MeV-1 TeV range. |b|>20°.

z/Classification	Number of sources
z	1534
No *z*	963
FSRQ	529
BL Lacs	1094
BCU	741
Others	133

Larger than any samples used to date for the determination of the blazar LF, broader extent of redshift. Would lead to remarkable improvement in LF determination

Marcotulli, L., Di Mauro, M. and Ajello, M., 2020. ApJ *896*(1), p.6.

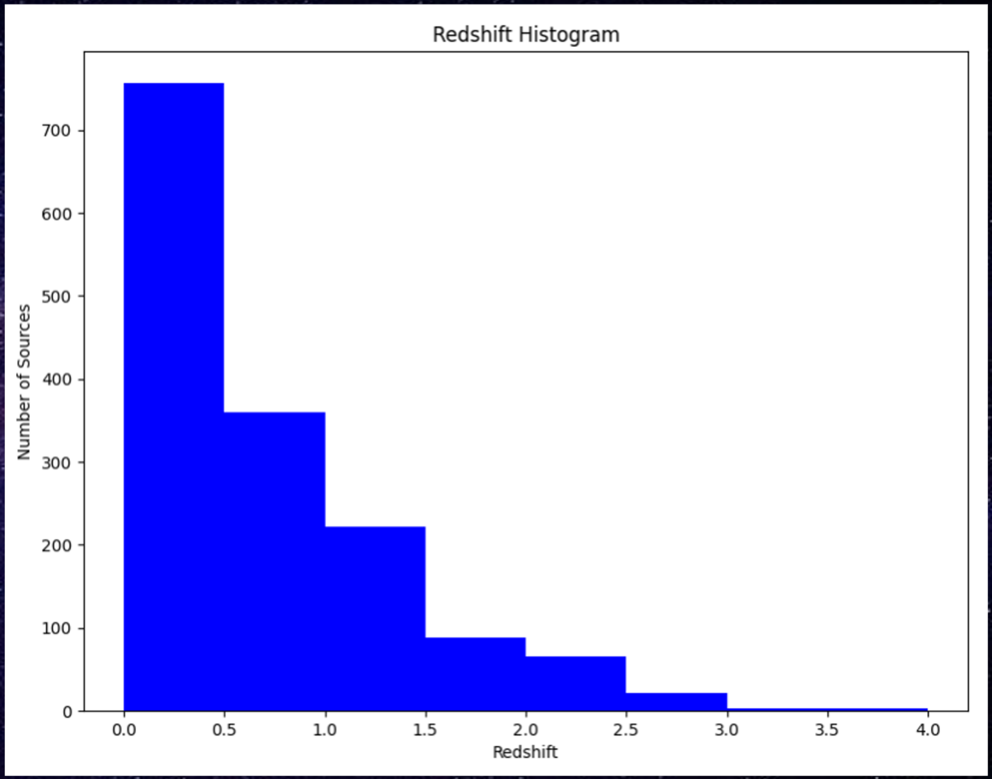

Understanding Evolution from Count Dataset

We can see the trend of enrollment for 4 different years.

On adding the total enrollment, we can see how the enrollment has changed over the years.

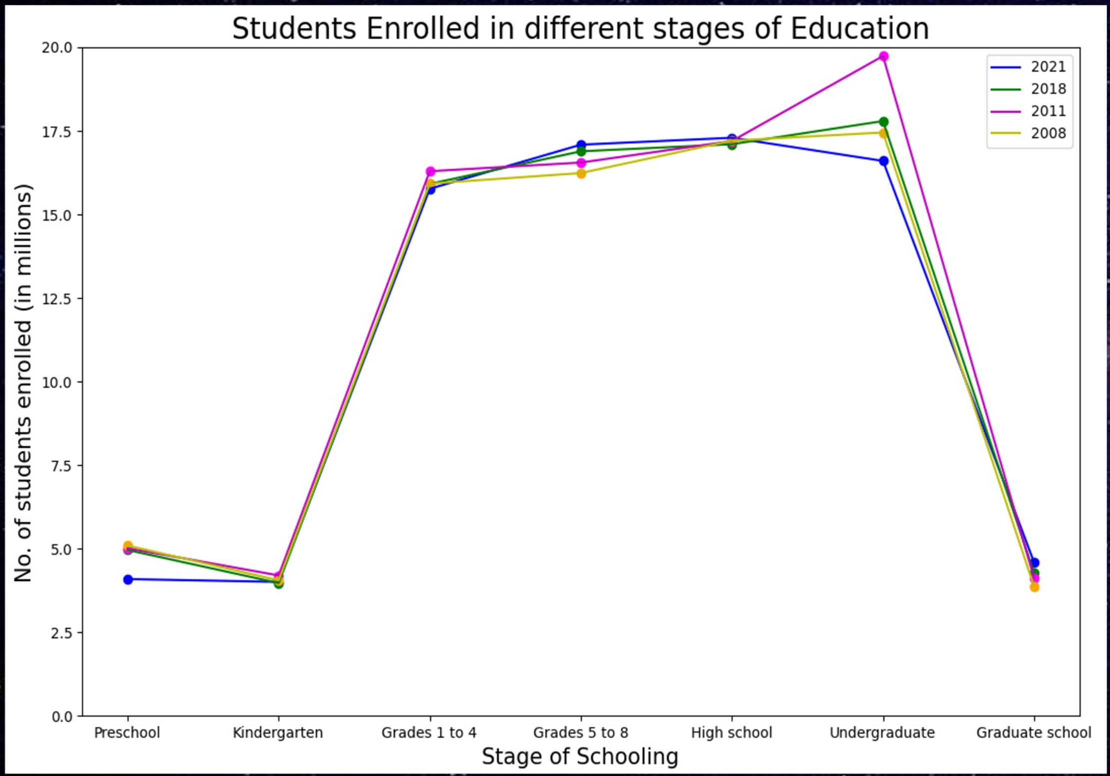

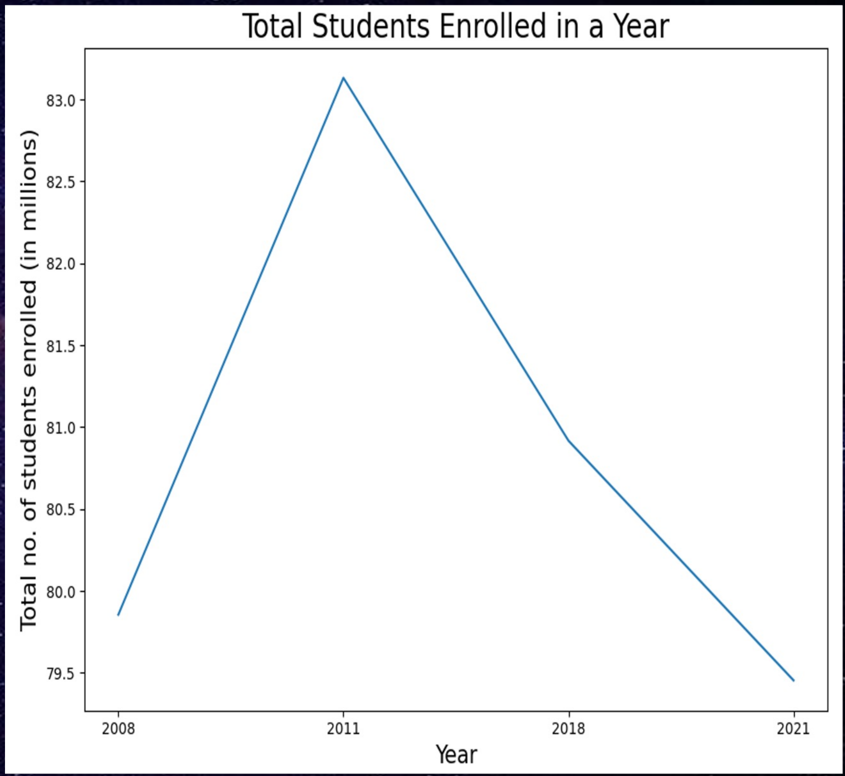

Data from: https://www.census.gov/library/publications/2003/dec/c2kbr-26.html

Evolution

Evolution: Shift of peak.

Major evolution at z~1.1

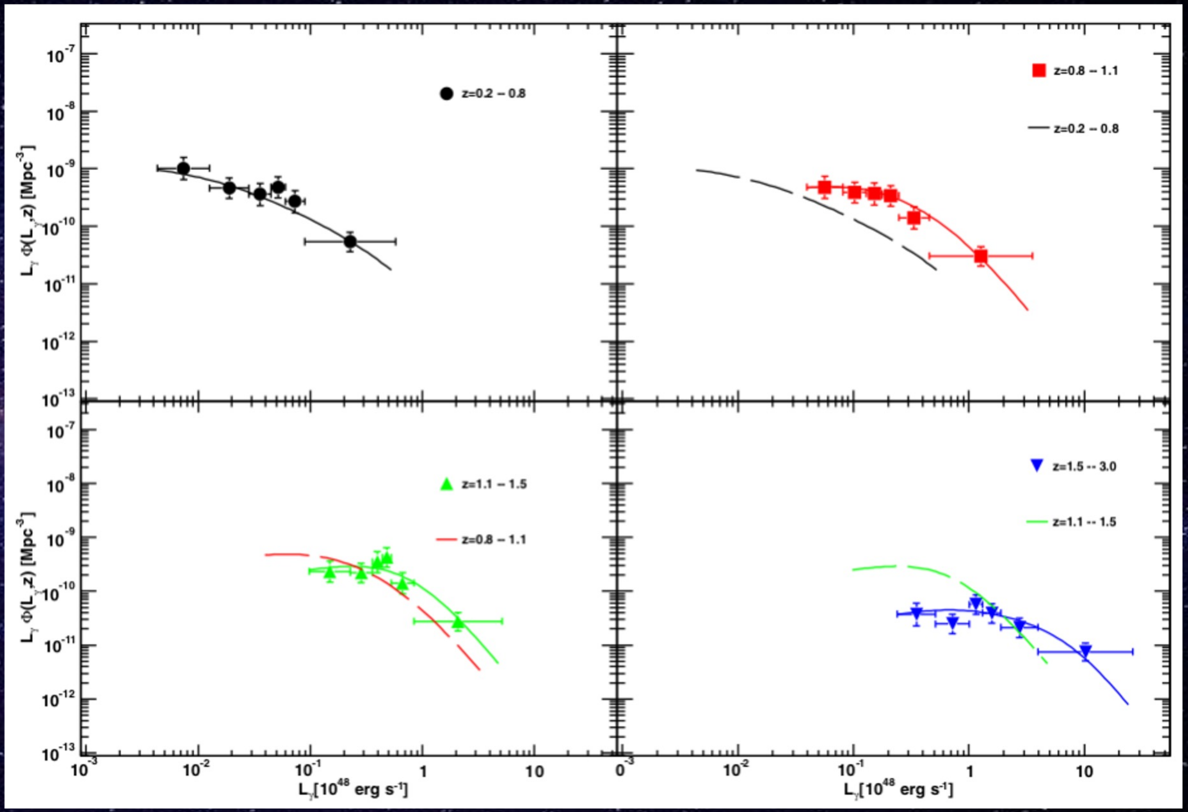

Luminosity Function of Blazars

- LF encodes evolution. Blazar LF is not well constrained.
- Blazars are good cosmological probes owing to their high luminosities and large redshifts.
- A major topic of debate is whether FSRQs and BL Lacs have the same evolution.
- Estimate the contribution of blazar emission to the extragalactic γ-ray background (EGB).

Cavaliere & D'Elia 2002.
Ajello et al. 2014.
Ajello et al. 2015.

Conclusion

- LF follows a double power-law shape.
- LF extends to 4 orders of magnitude lower in luminosities than previous studies.
- LF seems to be best represented by LDDE.
- Hint of a link between FSRQs and BL Lacs can be seen.
- Separate analysis of FSRQs and BL Lacs is required.